UiT
THE ARCTIC
UNIVERSITY
OF NORWAY

Faculty of Science and Technology
Department of Physics and Technology

Investigations of summer sea ice with X and C-band multi-polarimetric synthetic aperture radar (SAR)

—

Ane Schwenke Fors

A dissertation for the degree of Philosophiae Doctor – November 2016

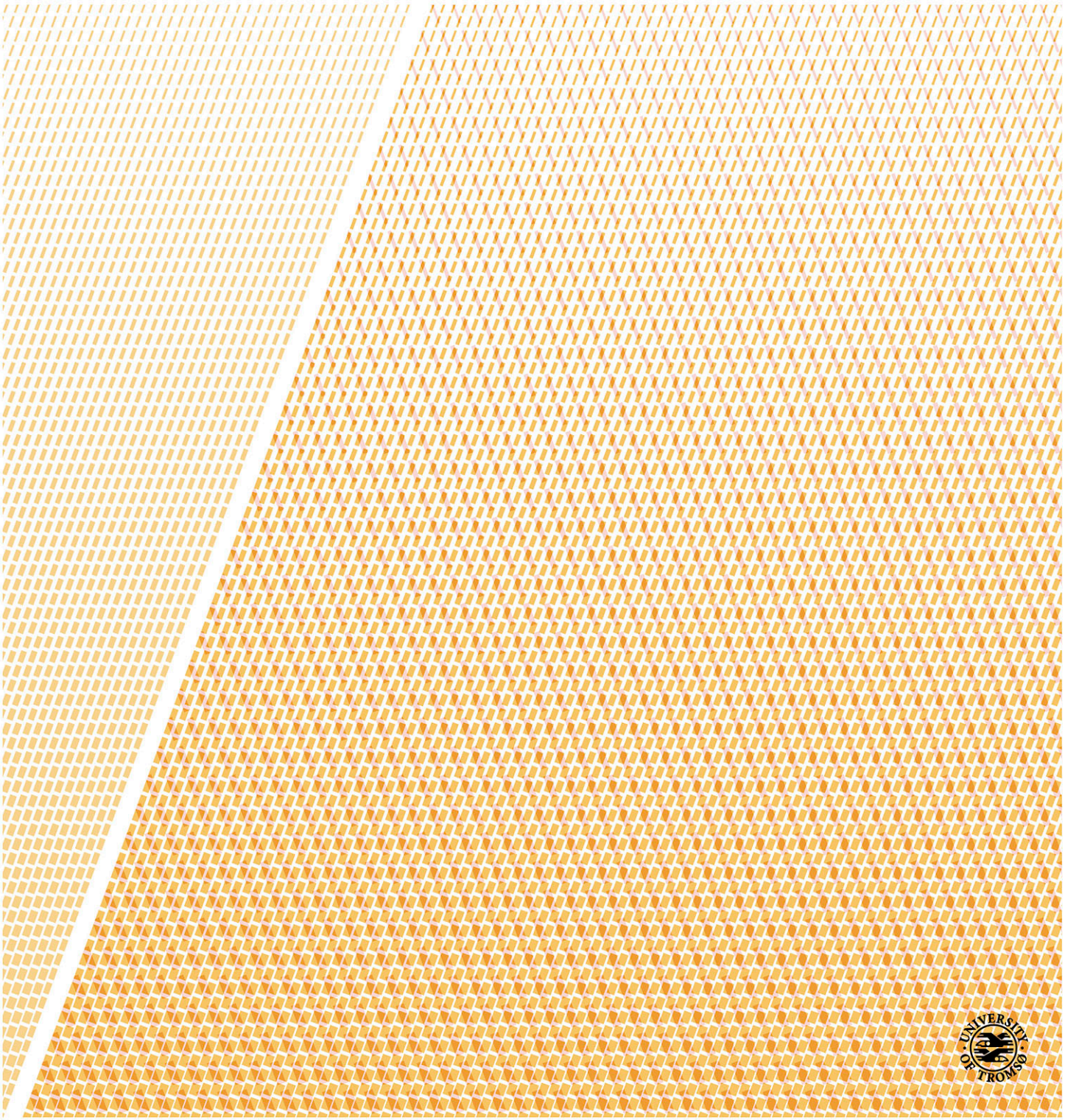

Abstract

Arctic sea ice is transforming towards a thinner, more seasonal, and more mobile sea ice cover with climate change. To better understand the observed changes, new and improved methods for monitoring of sea ice are required. Satellite synthetic aperture radar (SAR) is a useful tool for sea ice surveillance. In this thesis, we explore the possibilities and limitations of using space-borne multi-polarimetric SAR in summer sea ice investigations. Both X and C-band data are examined. The study utilizes two data sets collected in the Arctic in 2011 (Fram Strait) and 2012 (north of Spitsbergen). Both sets combine satellite SAR scenes with co-located ground and air-borne measurements.

Robust sea ice segmentation in SAR scenes is challenging, especially during summer melt. The sea ice type discrimination ability and temporal consistency of six polarimetric SAR features are examined to reveal their potential in summer sea ice segmentation. All SAR features are found to add value to sea ice type discrimination, and four of them perform consistently during changing meteorological conditions. An automatic segmentation algorithm based on the features is tested and evaluated. The algorithm succeeds in producing a good and temporally stable sea ice segmentation in C-band during changing conditions, but performs poorly in X-band. The poorer X-band performance could be related to frequency, lower incidence angles or fewer available polarisations. More information about how polarimetric SAR features relate to sea ice properties is necessary to develop the segmentation into a classification, labeling the segments.

Sea ice surface roughness influences the SAR signature of sea ice, but few studies have explored its influence on summer sea ice SAR imagery. The influence of large-scale sea ice surface roughness on different C-band polarimetric SAR features is here investigated during melt conditions. Several features are found related to macro-scale surface roughness, but the relationships are sensitive to incidence angle, meteorological conditions, and changes in micro-scale surface roughness. The interpretation of macro-scale surface roughness from the features improves with knowledge about meteorological conditions. The findings differ from previous studies in other seasons, demonstrating that SAR sea ice surface roughness signatures changes with season and sea ice type.

The presence and properties of melt ponds are also expected to strongly influence the sea ice SAR signature during summer. Relationships between melt pond fraction and several X-band polarimetric SAR features are here explored, and evaluated for their potential in melt pond fraction estimation. Wind speed and SAR incidence angle are found to have a large impact on the results.The findings imply that X-band possibly can be employed in addition to C-band for melt pond fraction estimation with SAR in the future, opening for extended monitoring of melt ponds from space.

Our study demonstrates new possibilities in segmentation and characterization of Arctic summer sea ice with multi-polarimetric satellite SAR. It highlights that information about weather and weather history is crucial for interpretation of SAR scenes during melt season. The findings contribute in the development of improved monitoring techniques for sea ice in a rapidly changing Arctic, increasing the safety of human activities and research in the ice-covered seas.

Acknowledgment

Foremost I wish to thank my supervisors for their support and guidance in the work of this thesis. Thanks to my main supervisor Torbjørn Eltoft for giving me the opportunity to start the Ph.D and for following me all through the journey. Thanks also to Anthony P. Doulgeris, taking over as my main supervisor in the completion phase, offering good and valuable discussions and solutions on small and large matters. I am grateful for all help and support from my co-supervisor Camilla Brekke, her presence, patience and advices brought me through the most difficult phases of my Ph.D. Finally, I want to thank my co-supervisor Sebastian Gerland at the Norwegian Polar Institute for shearing his knowledge and network of contacts, for his positive and encouraging attitude and for supporting my work through all stages of this project.

I acknowledge Regional Differensiert Arbeidsgiverafgift (RDA)-Troms County for financing my project, and hence allowing me to do this study. The project have also been supported finacially by the project "Sea Ice in the Arctic Ocean, Technology and Systems of Agreements" ("Arctic Ocean", subproject "CASPER") of the Fram Centre, and by the Centre for Ice, Climate and Ecosystems at the NPI.

Many scientists have also contributed to my work. I would like to thank my co-authors, Angelika H. H. Renner at the Institute of Marine Research, Justin F. Beckers at the University of Alberta and Dmitry V. Divine at the Norwegian Polar Institute for their help and inputs in the work with my papers. Stian N. Anfinsen at UiT- The Arctic University of Tromsø have also contributed with thoughts and ideas during this project. I would also like to acknowledge the crew of R/V Lance and the scientists participating in the Fram Strait 2011 and the ICE2012 campaigns for data collection and help with data access. The participants in the Tromsø-group of Sea Ice Remote Sensing have contributed with inspiration and inputs.

All my fellow Ph.D students and Post-Doc.s in the Earth Observation group have made my days happier during the work with this thesis, and contributed to a good working environment. A special thanks go to Stine Skrunes, Mari-Ann Moen and Malin Johansson. Thank you for cheering me up, supporting me whenever needed, and for sharing your everyday-life with me. I could not have made this without you.

My sincere gratitude goes to my family and friends for being there and encouraging me these years. Thanks to my parents for always believing in me and supporting me, and for looking after both me and my children whenever needed. Thanks to Eskil for his never-ending support and positive attitude, belaying me safe through my Ph.D. journey and life in general. Finally, thanks to my three main achievements during this period, Brage, Ingvild and Audun. You have brought my mind elsewhere every day, reminding me what life is really about.

I am gratefull to you all!

Ane Schwenke Fors,
Tromsø, November 2016

Contents

Abstract **i**

Acknowledgements **iii**

Table of Contents **vi**

Nomenclature **vii**
List of Notation vii
List of Acronyms ix

1 Introduction **1**
1.1 Motiviaton 1
1.2 Outline 2

2 Synthetic aperture radar (SAR) **3**
2.1 Frequency 3
2.2 Imaging geometry 4
2.3 Resolution 5
2.4 Speckle 7
2.5 Polarimetry 7
2.5.1 Scattering matrix 8
2.5.2 Scattering vectors 9
2.5.3 Covariance and coherency matrices 9
2.5.4 Polarimetric SAR features 10

3 Sea ice and SAR **11**
3.1 Sea ice 12
3.1.1 Growth, composition and seasonal evolution 12
3.1.2 Sea ice in a changing climate 14
3.2 Microwave properties of sea ice 15
3.3 SAR sensor parameters 17

4 Summer sea ice studies with SAR **19**
4.1 A brief review 19
4.2 Polarimetric SAR features 22

4.2.1 Statistical dependency 28

5 Study areas and data sets **29**
5.1 Fram Strait 2011 29
5.2 ICE 2012 30
5.3 Data material 30
5.3.1 Satellite scenes 31
5.3.2 Airborne and ground-based measurements 31
5.4 Challenges and limitations 34

6 Overview of Publications **37**
6.1 Paper summaries 37
6.2 Other publications and presentations 40

7 Paper 1:
Late summer sea ice segmentation with multi-polarisation SAR features in C- and X-band **43**

8 Paper 2:
Late summer Arctic Sea Ice Surface Roughness Signatures in C-Band SAR Data **61**

9 Paper 3:
Signature of Arctic first-year ice melt pond fraction in X-band SAR imagery **81**

10 Conclusions **105**
10.1 Research conclusions 105
10.2 Future outlook 106

Bibliography **119**

Nomenclature

List of Notation

A	anisotropy
B	bandwidth
c	speed of light
$\boldsymbol{C}$	covariance matrix
d	number of polarimetric channels
d_a	synthetic aperture length
DoP	degree of polarisation
$\boldsymbol{e_i}$	i^{th} eigenvector of $\boldsymbol{T}$
E_p^i	electromagnetic field of the incident wave in polarisation p
E_p^s	electromagnetic field of the scattered wave in polarisation p
GB	geometric brightness
H	entropy
H'	entropy in dual-polarimetric case
k	wave number
$\boldsymbol{k}$	Pauli scattering vector
L_a	antenna length
p_i	probability of the i^{th} scattering mechanism
P_D	Freeman-Durden, double-bounce scattering component
P_S	Freeman-Durden, surface scattering component
P_V	Freeman-Durden, volume scattering component
PH	pedestal height
r	Spearmans' correlation coefficient
r_a	azimuth resolution, SAR
r_g	ground range resolution
r_s	slant range resolution
R	distance from sensor to target
$R_{HV/HH}$	cross-polarisation ratio
$R_{VH/VV}$	cross-polarisation ratio
$R_{VV/HH}$	co-polarisation ratio
RK	relative kurtosis
s_{rms}	root mean square height

$\boldsymbol{s}$	lexicographic scattering vector
S_{pq}	complex scattering coefficient of transmit polarisation p and receive polarisation q
$\boldsymbol{S}$	scattering matrix
$SPAN$	span of $\boldsymbol{C}$
$\boldsymbol{T}$	coherency matrix
x_a	azimuth resolution, radar
$\bar{\alpha}$	mean scattering angle
α_i	scattering angle of the the i^{th} eigenvector
α_i'	scattering angle of the the i^{th} eigenvector in the dual-polarisation case
ϵ	relative permittivity
θ	incidence angle
θ_a	azimuth beam width
λ	wavelength
λ_i	i^{th} eigenvalue of $\boldsymbol{T}$
ρ	co-polarisation correlation coefficient
ρ_{RRLL}	circular co-polarisation coefficient
σ^0	radar backscatter intensity
τ	pulse time length
ϕ_{pq}	phase of the complex scattering coefficient of transmit polarisation p and receive polarisation q
$()^\dagger$	transpose
$()^*$	complex conjugate
$()^{*\dagger}$	Hermitian transpose
$\langle\cdot\rangle$	sample mean

List of Acronyms

CAA	Canadian Arctic Archipelago
CCRS/CCT	Canadian Centre for Remote Sensing
CIA	center incidence angle
DTM	digital terrain model
EM	electromagnetic
GPS	global positioning system
FYI	first-year sea ice
INS	inertial navigation system
MAP	maximum a posteriori
MLC	multilook complex
MYI	multiyear sea ice
NESZ	noise equivalent sigma zero
NPI	Norwegian Polar Institute
PDF	probability density function
RCM	RADARSAT Constellation Mission
SAR	synthetic aperture radar
SLC	single-look complex
SPM	small perturbation model
WMO	World Meteorological Organization

Chapter 1

Introduction

This thesis explores the potential in using multi-polarisation satellite SAR imagey for segmentation and characterization of Arctic sea ice in the summer season, combining SAR scenes with co-located ground and air-borne measurements. The following sections present the motivation and the outline of the study.

1.1 Motiviaton

Arctic sea ice is changing with climate change. The sea ice extent, thickness and volume have reduced during the last decades [Kwok et al., 2009; Laxon et al., 2013; Parkinson and Comiso, 2013], and the length of the melt season have been increasing with a rate of about five days per decade since 1979 [Stroeve et al., 2014]. We see a shift towards a thinner, more seasonal and more mobile sea ice cover [Perovich et al., 2015]. The changes happen faster than models have projected [Meier et al., 2014; Stroeve et al., 2012], and there is a need for more and improved information about the Arctic sea ice to better understand the processes governing these changes. Improved sea ice monitoring would also increase the safety of human activities and research in the Arctic ice-covered seas [Eicken, 2013]. Collecting data from the Arctic is challenging. The area is remote, with harsh weather conditions and no daylight during many months of the year. Ground based campaigns are expensive and can only cover a small geographic area at the time. Remote sensing offers larger spatial coverage, but the lack of sunlight during parts of the year, and the persistent cloud cover in the area limit the use of many instruments. Use of the satellite data is also dependent on *in-situ* measurements for validation.

Spaceborne synthetic aperture radar (SAR) is an active microwave satellite instrument that can be used independent of daylight and cloud cover. Operational sea ice services around the world use SAR scenes as their main source for sea ice extent and concentration mapping [Moen et al., 2013]. For operational use, single and dual-polarisation modes are preferred over quad-polarisation scenes due to their wider spatial coverage and better revisiting frequency. However, SAR scenes acquired in quad-polarisation modes can give more detailed information about sea ice properties, and have higher spatial

resolution. They can therefore be utilized to explore the possibilities and limitations of sea ice information retrieval from SAR [Drinkwater et al., 1992; Scheuchl et al., 2004].

The behavior of microwave scattering in sea ice is extremely complicated, and interpretation of the SAR signal is not straightforward. It requires detailed knowledge about sea ice properties and their interaction with the radar wave [Dierking, 2013]. Research on sea ice and SAR has been ongoing for several decades, but a majority of the studies has focused on the winter season. Wet snow , freeze and melt cycles, and the presence of melt ponds on the sea ice surface make SAR investigations of summer sea ice challenging [Onstott, 1992; Scharien et al., 2012]. Nevertheless, the recent shift towards a longer melt season and more seasonal Arctic sea ice raise the importance of sea ice information retrieval during summer.

The aim of this thesis is to improve the understanding and interpretation of Arctic summer sea ice in SAR satellite scenes. The study is based on multi-polarimetric SAR scenes in X and C-band combined with ground and air-borne measurements. The thesis focuses on three main research questions:

- Is it possible to segment different sea ice types in late summer SAR scenes, and how are changing temperatures and sea ice conditions affecting the segmentation outcome? (Paper I)
- How is macro-scale sea ice surface roughness influencing SAR imagery in summer season, and can individual polarimetric SAR features be used to describe surface roughness? (Paper II)
- Which polarimetric SAR features are sensitive to melt pond fraction, and can we estimate melt pond fraction from X-band SAR scenes? (Paper III)

1.2 Outline

This thesis organizes as follows. Chapter 2 presents an overview of the basic principles and properties of SAR sensors. Chapter 3 gives an introduction to sea ice, describes its microwave properties, and discusses the role of SAR sensor parameters in sea ice monitoring. A deeper insight into summer sea ice SAR investigations is given in Chapter 4. Chapter 5 describes the study areas and data sets utilized in the thesis. A summary of the research publication included in the thesis is found in Chapter 6, whereas the full papers are presented in Chapters 7-9. Chapter 10 provides research conclusions and outlook.

Chapter 2

Synthetic aperture radar (SAR)

SAR is an imaging sensor, transmitting electromagnetic (EM) pulses and recording the returned echo, or *backscattered* signal. Based on the round-trip time of the pulse, the distance to the target can be estimated from the known speed of light. SAR operates in the microwave region of the EM specter, and the backscatter will depend on the dielectric and geometrical properties of the investigated surface. The surface' geophysical properties can be estimated by using post-processing techniques [van Zyl and Kim, 2011]. SAR is an active sensor, providing its own illumination source, and can therefore operate without daylight. Microwaves can also penetrate clouds and rain, making SAR almost weather independent. These properties make SAR a highly relevant instrument for Arctic sea ice surveillance. The following sections will introduce the basic principles of SAR imaging, needed to understand the theoretical basis of Paper I-III.

2.1 Frequency

SAR systems are assigned to different frequencies (see Table 2.1). In SAR monitoring of sea ice, C-band has long been the preferred frequency, but Ku, X and L-band are also used [Dierking, 2013]. This thesis investigates sea ice summer signatures in X (Paper I and III) and C- band (Paper I and II). The effect of frequency in SAR imaging of sea ice is further discussed in Sec. 3.2.

Table 2.1: Commonly used frequency bands for SAR [Moreira et al., 2013].

Frequency band	**Ka**	**Ku**	**X**	**C**	**S**	**L**	**P**
Frequency (GHz)	40-25	17.6-12	12-7.5	7.5-3.75	3.75-2	2-1	0-5-0.25
Wavelength (cm)	0.75-1.2	1.7-2.5	2.5-4	4-8	8-15	15-30	60-120

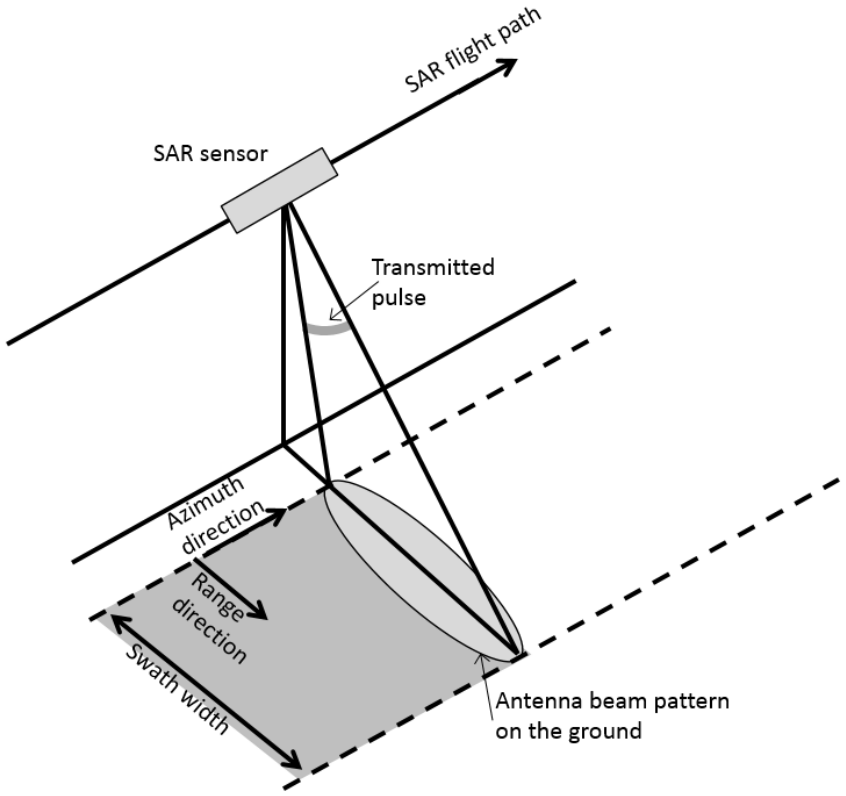

Figure 2.1: Imaging geometry for a SAR. Figure from Skrunes [2014].

2.2 Imaging geometry

A SAR system is usually mounted on a moving platform in form of an aircraft or, as in our study, a satellite. The system is side-looking with the platform moving in the *azimuth* direction, aiming the antenna in the *range* direction, perpendicular to the flight direction (see Fig. 2.1). The illuminated area at ground is termed swath, and the coverage in range direction is called *swath width*.

Range is commonly measured in two different ways. *Slant range* refers to the range along the radar line of site, as illustrated in Fig. 2.2. On the other hand *ground range* refers to the range along the ground measured from nadir, resulting in a correct geometry relative to a map projection. Slant range and ground range are connected through the *incidence angle*, defined as the angle between the radar beam and the normal to the surface [Oliver and Quegan, 2004].

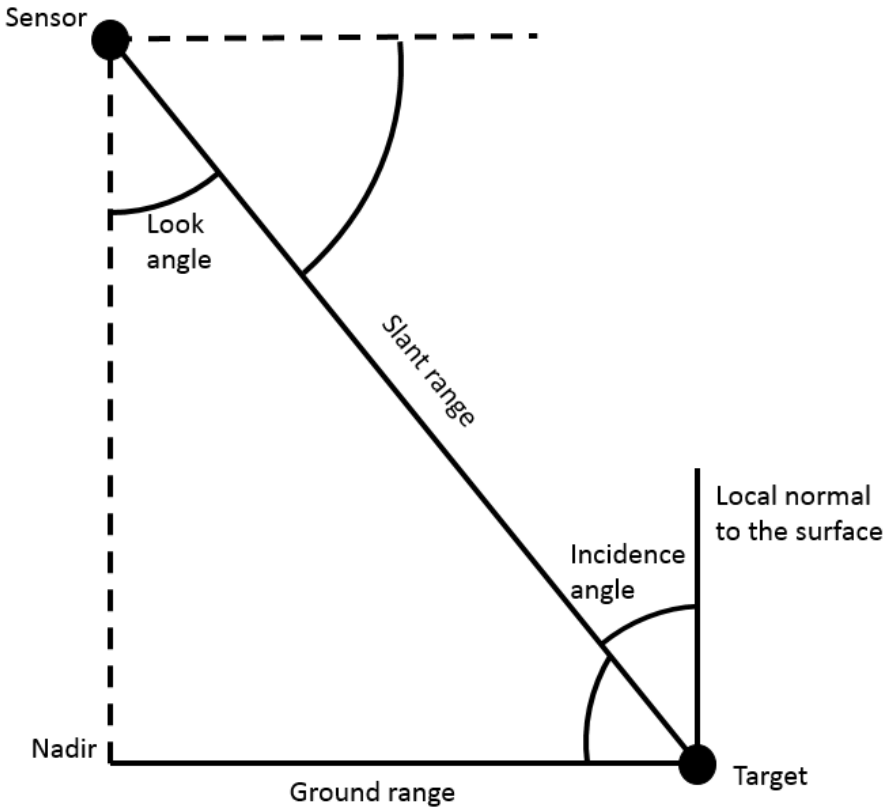

Figure 2.2: Definition of some common radar imaging terms. Figure from Skrunes [2014].

2.3 Resolution

The resolution of an image is the minimum distance two objects can have, allowing them to be resolved in the final image. If the distance is smaller, their reflections will overlap, and they could not be separated in the image. The slant range resolution (r_s) can be written as

$$r_s = \frac{c}{2B}, \tag{2.1}$$

where c is the speed of light, B is the pulse bandwidth given as $B = \frac{1}{\tau}$, and τ is the pulse length [van Zyl and Kim, 2011]. The factor of two is due to the two-way travel of the pulse. To enhance the signal-to-noise ratio, each pulse should contain as much energy as possible. This can be solved with a longer pulse, but this would hamper the resolution. To achieve both a longer pulse and an acceptable resolution, a chirp pulse, which is a frequency modulated pulse, can be used. This technique gives a wide bandwidth even when the pulse is long [van Zyl and Kim, 2011]. The ground range resolution (r_g) can be

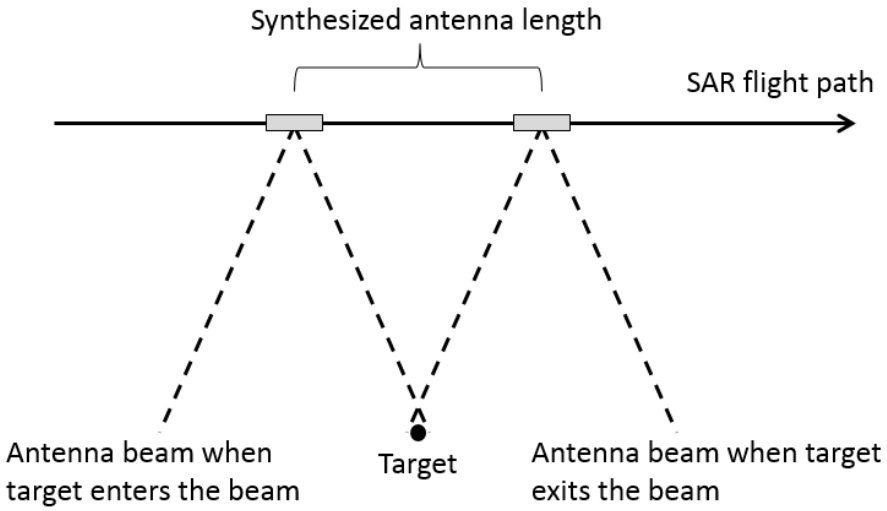

Figure 2.3: The SAR principle. High resolution is achived by using the forward motion of the sensor to synthesize a longer antenna. Figure from Skrunes [2014].

retrieved from r_s by using the incidence angle (θ), and is given as

$$r_g = \frac{r_s}{\sin\theta}, \tag{2.2}$$

using flat earth approximation [van Zyl and Kim, 2011]. It will hence vary with incidence angle across the swath width.

In a real-aperture radar system, azimuth resolution (x_a) is based on the azimuth beam-width (θ_a), dependent on the antenna length (L_a) and the radar wavelength (λ). It can be written as

$$x_a \approx R\theta_a \approx \frac{R\lambda}{L_a}, \tag{2.3}$$

where R is the distance between the antenna and the target [van Zyl and Kim, 2011]. The resolution can hence be improved by increasing the antenna length or reducing the distance to the target. Both of these solutions are inconvenient for spaceborne sensors. To overcome the physical limitations of increasing the antenna length, the motion of the radar antenna can be used to simulate a large synthetic antenna, as shown in Fig. 2.3. A number of pulses from different azimuth angles hit a target at the surface as the radar passes over it. Advanced signal processing is used to combine the pulses into an image with improved azimuth resolution (r_a), given as

$$r_a = \frac{d_a}{2}, \tag{2.4}$$

where the synthetic aperture length (d_a) equals the length of the sensor path during the time the target stays in the beam [van Zyl and Kim, 2011]. Equation 2.4 displays the magic of SAR; the azimuth resolution is independent of the distance between the sensor

and the surface. The above equation assumes a fixed antenna. An even higher resolution can be achieved with a steered beam, but this will be at the expense of spatial coverage [Oliver and Quegan, 2004].

2.4 Speckle

SAR images have a granular noise pattern, often described as "salt and pepper" noise. This noise-like behavior, termed *speckle*, is an inherent property in all coherent imaging systems. Speckle arises from constructive and destructive interference between the large number of individual scatterers that exist within a resolution cell. Hence, it is not only noise, but also carries information [Oliver and Quegan, 2004]. Speckle in SAR images complicates image analysis and interpretation, and reduces the effectiveness of segmentation and classification [Lee and Pottier, 2009]. *Multilooking* is therefore commonly applied for speckle reduction. It can be applied during image formation by dividing the aperture length into several *looks* and average these, but more often multilooking is performed by averaging neighboring single-look pixels in the spatial domain [Lee and Pottier, 2009; Oliver and Quegan, 2004]. Several different filter types have been developed for speckle reduction [Lee and Pottier, 2009].

2.5 Polarimetry

SAR polarimetry offers extended physical information about a surface, and has a wide range of applications [Lee and Pottier, 2009; Moreira et al., 2013]. This thesis explores the advantages of polarimetry in summer sea ice investigations, and a profound understanding of polarimetry is hence important to understand both the theory, method and results of Paper I-III. Polarimetry is based on the possibility of combining EM waves with different polarisations to investigate the properties of a surface. An EM wave consists of electric and magnetic fields, which oscillate orthogonal to each other and to the direction of energy propagation. The *polarisation* of an EM wave describes the orientation of its oscillations, or the shape of the pattern traced by the tip of the electric field [van Zyl and Kim, 2011].

Quad-polarised SAR systems transmit and receive both *horizontally* (H) and *vertically* (V) linearly polarised waves (see Fig. 2.4). This result in a four-channel combination, consisting of HH, HV, VH, and VV, where the first and the second letter refers to the transmitted and received waves, respectively. These systems are often referred to as *fully polarised* systems, and any polarisation can be synthesized from them. In some cases, the relative *phase* between the channels is also retrieved, giving additional information about the investigated surface. *Dual-polarised* SAR systems can either transmit one polarisation and receive two orthogonal polarisations (HH-HV or VV-VH), or alternate the transmission polarisation to obtain co-polarised orthogonal measurements (HH-VV). In the simple case of *single-polarisation*, the SAR system transmits and receives the same polarisation

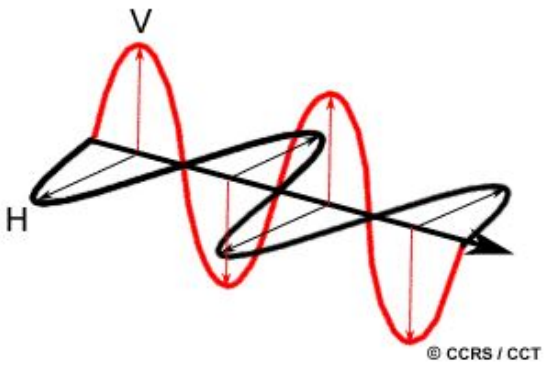

Figure 2.4: EM waves with horizontal (black) and vertical (red) polarisations. Figure from Canada Centre for Mapping and Earth Observation [2015].

(HH or VV) [Moreira et al., 2013; van Zyl and Kim, 2011]. *Multi-polarisation* is a common term used in cases with more than one polarisation channel. In the newly developed field of compact polarimetry, circular polarisation is also utilized in combination with linearly received waves [Raney, 2011]. The following subsections present the mathematical representations of linear orthogonally polarised data.

2.5.1 Scattering matrix

In the quad-polarimetric case, a 2×2 matrix of *complex scattering coefficients* (S_{xx}) is produced for each pixel, describing the scattering process in the corresponding area at the surface. This *scattering matrix* ($\boldsymbol{S}$) describes the transformation of the incident electric field (E^i) to the scattered electric field (E^s) by

$$\begin{bmatrix} E_x^s \\ E_y^s \end{bmatrix} = \frac{e^{-jkR}}{R} \begin{bmatrix} S_{pp} & S_{qp} \\ S_{pq} & S_{qq} \end{bmatrix} \begin{bmatrix} E_x^i \\ E_y^i \end{bmatrix}, \tag{2.5}$$

where k is the wave number and R is the distance between radar and target [Lee and Pottier, 2009]. p and q represents the orthogonal polarisations, and the first and second subscripts of the complex scattering coefficients refer to the transmitted and received polarisations, respectively. In the following, the polarisations are restricted to the linear horizontal-vertical basis ($p, q \in H, V$). The scattering matrix is then written as

$$\boldsymbol{S} = \begin{bmatrix} S_{HH} & S_{VH} \\ S_{HV} & S_{VV} \end{bmatrix} = \begin{bmatrix} |S_{HH}|e^{j\phi_{HH}} & |S_{VH}|e^{j\phi_{VH}} \\ |S_{HV}|e^{j\phi_{HV}} & |S_{VV}|e^{j\phi_{VV}} \end{bmatrix}, \tag{2.6}$$

where $|S_{xx}|$ and ϕ_{xx} denotes the amplitudes and phases of the complex scattering coefficients [Lee and Pottier, 2009]. The diagonal elements of $\boldsymbol{S}$ represent the *co-polarisation* channels, while the off-diagonal elements represent the *cross-polarisation* channels. In the monostatic case, where the transmit and receive antenna are co-located, $\boldsymbol{S}$ is known as

the *Sinclair matrix*. *Reciprocity* ($S_{HV} = S_{VH}$) can then be assumed [Lee and Pottier, 2009; Oliver and Quegan, 2004].

2.5.2 Scattering vectors

The scattering matrix can also be represented in vectorised versions. Assuming reciprocity, the *lexicographic basis scattering vector* ($\boldsymbol{s}$) is defined as

$$\boldsymbol{s} = \begin{bmatrix} S_{HH} & S_{HV} & S_{HV} \end{bmatrix}^{\dagger}, \tag{2.7}$$

where † denotes the transpose [Lee and Pottier, 2009]. In this case, the vector elements represent the coefficients of the Lexicographic decomposition of $\boldsymbol{S}$.

Another representation of $\boldsymbol{S}$ is the *Pauli basis scattering vector* ($\boldsymbol{k}$), written as

$$\boldsymbol{k} = \frac{1}{\sqrt{2}} \begin{bmatrix} S_{HH} + S_{VV} & S_{HH} - S_{VV} & 2S_{HV} \end{bmatrix}^{\dagger}. \tag{2.8}$$

The vector elements are the coefficients in the Pauli decomposition of $\boldsymbol{S}$, and are expected to represent different scattering mechanisms [Lee and Pottier, 2009]. In the dual-polarimetric case, the scattering vectors reduce to two-element vectors.

2.5.3 Covariance and coherency matrices

The scattering matrix and scattering vectors are *single look complex* (SLC) measurements (see Sec. 2.4). Advancing to *multilook complex* (MLC) data can be done through spatial multilooking. The scattering vectors can be multilooked by computing their sample *covariance matrix* ($\boldsymbol{C}$) or *coherency matrix* ($\boldsymbol{T}$). These matrices are formed from the mean Hermitian outer product of the lexicographic and Pauli basis scattering vectors, respectively. They can be written as

$$\boldsymbol{C} = \frac{1}{L} \sum_{i=1}^{L} \boldsymbol{s}_i \boldsymbol{s}_i^{*\dagger}, \tag{2.9}$$

and

$$\boldsymbol{T} = \frac{1}{L} \sum_{i=1}^{L} \boldsymbol{k}_i \boldsymbol{k}_i^{*\dagger}, \tag{2.10}$$

where $\boldsymbol{s}_i$ and $\boldsymbol{k}_i$ are the SLC scattering vectors corresponding to pixel i, L is the number of scattering vectors included in the averaging, and * denotes the complex conjugate [Lee and Pottier, 2009]. In the quad-polarimetric case (assuming reciprocity), $\boldsymbol{S}$ and $\boldsymbol{T}$ are given by

$$\boldsymbol{C} = \begin{bmatrix} \langle |S_{HH}|^2 \rangle & \sqrt{2}\langle S_{HH} S_{VH}^* \rangle & \langle S_{HH} S_{VV}^* \rangle \\ \sqrt{2}\langle S_{VH} S_{HH}^* \rangle & 2\langle |S_{VH}|^2 \rangle & \sqrt{2}\langle S_{VH} S_{VV}^* \rangle \\ \langle S_{VV} S_{HH}^* \rangle & \sqrt{2}\langle S_{VV} S_{VH}^* \rangle & \langle |S_{VV}|^2 \rangle \end{bmatrix}, \tag{2.11}$$

and

$$\boldsymbol{T} = \frac{1}{2}\begin{bmatrix} \langle|S_{HH}+S_{VV}|^2\rangle & \langle(S_{HH}+S_{VV})(S_{HH}-S_{VV})^*\rangle & 2\langle(S_{HH}+S_{VV})S_{VH}^*\rangle \\ \langle(S_{HH}-S_{VV})(S_{HH}+S_{VV})^*\rangle & \langle|S_{HH}-S_{VV}|^2\rangle & 2\langle(S_{HH}-S_{VV})S_{VH}^*\rangle \\ 2\langle S_{VH}(S_{HH}+S_{VV})^*\rangle & 2\langle S_{VH}(S_{HH}-S_{VV})^*\rangle & 4\langle|S_{VH}|^2\rangle \end{bmatrix}, \quad (2.12)$$

where the $\langle\cdot\rangle$ indicate ensemble averaging. $\boldsymbol{C}$ and $\boldsymbol{T}$ are related through a simple unitary transformation, and they have identical eigenvalues. In the dual-polarimetric case, $\boldsymbol{C}$ and $\boldsymbol{T}$ reduce to 2×2 matrices.

The multilook process could be performed either using a sliding or stepping averaging window. With a sliding window, the window is shifted one pixel prior to each averaging, while the stepping window is shifted the width of the window. A sliding window preserves the number of pixels, but neighboring pixels will be highly correlated. A stepping window reduces the number of pixels, but speeds up the multilook process.

2.5.4 Polarimetric SAR features

Various *polarimetric SAR features* can be extracted from the covariance and coherency matrices. The polarimetric features can be used for identification of scattering mechanisms, and for retrieval of information about physical properties of the observed surfaces. Some polarimetric features can be directly retrieved from the MLC matrices or from ratios of their elements. Others can be retrieved from *polarimetric decompositions* of the matrices, including model-based decompositions and decompositions using eigenvector or eigenvalue analysis [Lee and Pottier, 2009]. *Textural features* explore the statistical properties from a neighborhood of pixels. In this thesis SAR features are used to represent polarimetric SAR imagery information. A review of the features utilize in Paper I-III is presented in Sec. 4.2.

Chapter 3

Sea ice and SAR

Satellite SAR is highly valuable for sea ice monitoring, due to its independence of daylight and cloud coverage. Operational sea ice services are dependent on SAR in producing sea ice concentration maps; the Canadian Ice Service alone processes more than ten thousand SAR scenes every year [Moen et al., 2013]. SAR scenes are also used for monitoring sea ice extent, sea ice drift and deformation, basic ice type classification, determination of melt onset and freeze-up, and to some degree for estimation of sea ice thickness. In science applications, local and regional observations of sea ice deformation, sea ice growth and sea ice melt can be performed with SAR. It can also be used to validate results from models and for quality assessments of coarse-resolution spaceborne instruments, e.g., microwave radiometers and scatterometers [Breivik et al., 2009; Dierking, 2013]. SAR information extraction from summer sea ice is an ongoing challenge, and is further discussed in Chapter 4.

C-band SAR satellites have for a long time been preferred for operational sea ice monitoring. At present, the Canadian RADARSAT-2 and the European Sentinel-1a satellites cover the sea ice services' main needs. Other frequencies can offer additional information about sea ice, ALOS/PALSAR-2 (L-band) and TerraSAR-X (X-band) represents the leading supplement to C-band in SAR sea ice investigations. In the future, SAR constellation missions, such as Sentinel-1 (a and b) and RADARSAT Constellation Mission (RCM), will increase the spatial and temporal sampling possibilities [Arkett et al., 2015; Torres et al., 2012]. Development of compact polarimetry, and fully polarimetric scenes with wide swath width, will also provide new opportunities in full polarimetric sea ice monitoring [Espeseth et al., 2016; Geldsetzer et al., 2015; Villano et al., 2014]. This implies a demand for more studies on polarimetric signatures of sea ice.

An introduction to sea ice, its microwave properties and the effect of sensor parameters on SAR sea ice imagery is given in the following sections, introducing concepts important for the interpretation of the results presented in Paper I-III.

3.1 Sea ice

Approximately 10% of the world's oceans is covered by sea ice [Shokr and Nirmal, 2015]. It is a very complex medium, continuously modified by winds, currents, and air and ocean temperature fluctuations. Most sea ice occurs as *drift ice*, moving freely with currents and winds. *Fast ice* on the other hand, is immobile ice either attached to the shore or seafloor or locked between grounded icebergs.

A common sea ice nomenclature based on age and thickness of the ice is developed by the World Meteorological Organization [WMO, 2014]. It divides sea ice into the stages of *new ice*, *nilas*, *pancake ice*, *young ice*, *first-year ice (FYI)* and *old ice*, each with several subclasses (see Table 3.1 and Fig. 3.1). The work presented in these thesis focuses on FYI (Paper I, II and III) and old ice (Paper I and II). FYI is by WMO defined as sea ice thicker than 30 cm, that is not more than one winter old. Old ice, in the following also referred to as *multiyear ice* (MYI), has on the other hand survived at least one summer's melt.

Table 3.1: WMO sea ice classes [WMO, 2014].

Sea ice class	**Properties**	**Thickness**
New ice (*Frazil ice, grease ice, slush, shuga*)	Recently formed sea ice, not yet solid	-
Nilas (*Dark nilas, light nilas, ice rind*)	Thin elastic crust of ice, easily bending on waves and swell	< 0.1 m
Pancake ice	Circular pieces of ice with raised rims due to the pieces striking each other	< 0.1 m
Young ice (*Grey ice, grey-white ice*)	Ice in the transition stage between nilas and first-year ice	$0.1 - 0.3$ m
First-year ice (*Thin, medium and thick first-year ice*)	Sea ice of not more than one winter's growth	0.3 - 2 m
Old ice (*Residual ice, second and multi-year ice*)	Sea ice which has survived at least one summer's melt	~ 2 m

3.1.1 Growth, composition and seasonal evolution

Sea ice forms from freezing seawater, when the top layer of the water cools to about $-1.8°C$, depending on its salinity. Its initial form depends on the sea state, wind, and temperature at the time of formation. Some of the seawater salt is included in the sea ice volume as *brine* during sea ice formation. The amount of brine trapped depends on the growth rate of the sea ice, which is higher at low temperatures, and therefore most prominent in the top sea ice layer. After the initial entrapment, brine expulsion

(a) New ice.

(b) Pancake ice.

(c) Young ice with finger rafts.

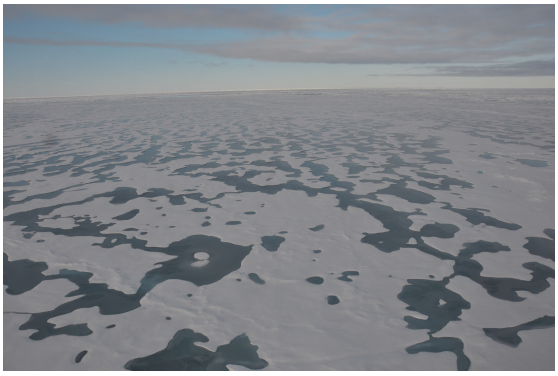

(d) Summer first-year ice.

(e) Summer multiyear ice with melt ponds.

Figure 3.1: Example photos of different sea ice types. Image courtesy of A. H. H. Renner.

and gravity drainage lead to a reduction in brine volume with age. *Air bubbles* are also entrapped in the ice during ice formation, and their volume increases as the brine drainage leaves empty cavities and drainage channels in the sea ice [Petrich and Eicken, 2009; Tucker et al., 1992].

Rises in temperature, and melt water forming from melting snow and sea ice, change

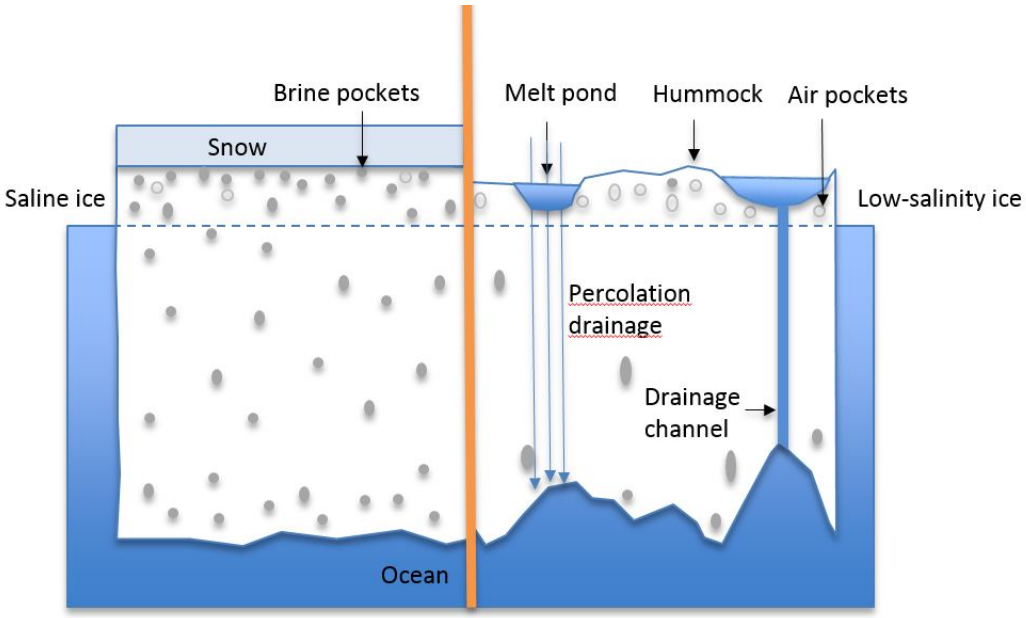

Figure 3.2: Schematic draw of winter first-year ice (left) and late summer first-year ice (right), illustrating differences in the top layer of the ice.

the properties of sea ice during the melt season. The sea ice *salinity* decreases due to increasing temperatures and melt water flushing. Warming of the sea ice also leads to re-texturing of the sea ice structure, and freeze and thaw cycles can lead to superimposed ice at the sea ice surface [Petrich and Eicken, 2009; Scharien et al., 2010; Tucker et al., 1992]. *Melt ponds* form at the sea ice surface from melt water, changing its properties and the surface albedo. Their surface coverage vary rapidly during the melt season, and can reach up to $50 - 60\%$ in early summer. As the summer season proceeds, the ponds drain through melt channels and percolation through the sea ice, reducing their coverage. In early autumn, the ponds begin to refreeze [Eicken et al., 2004; Perovich, 2002; Polashenski et al., 2012]. Melt ponds are the main focus of Paper III.

At the end of the melt season, new ice growth starts, and the FYI that survived the summer melt is termed MYI. MYI is characterized by lower salinity and density than FYI. Its surface topography has a smoothed undulating appearance, with low areas formed by melt ponds and adjacent *hummocks*, whereas FYI is mainly flat, disrupted by deformed areas of ridges with distinct collections of angular blocs [Tucker et al., 1992]. Figure 3.2 give a schematic sketch of FYI during winter and summer conditions, illustrating differences in the top layer of the ice.

3.1.2 Sea ice in a changing climate

Changes in sea ice extent and volume are important indicators of climate change. As stated in Chapter 1, a large decline in sea ice cover and a lengthening of the melt season

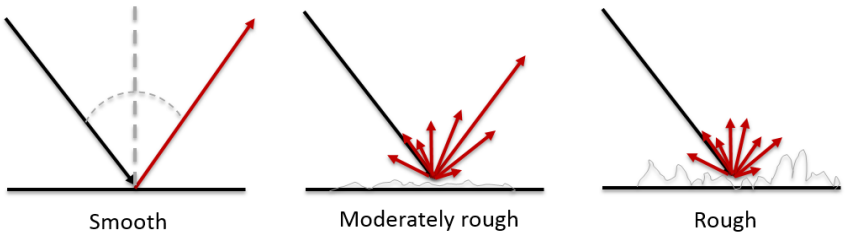

Figure 3.3: Schematic figure of radar backscatter for a smooth, moderately rough and rough surface. The black arrows represent the incident radar signal, and the scattered signal is displayed in red.

has been observed during the last decades. In the coming decades, we could possibly experience a near ice-free Arctic during summer [Meier et al., 2014]. The observed changes leads to a shift in ice regimes towards less MYI and more seasonal FYI, making monitoring of summer sea ice increasingly important [Perovich et al., 2015].

3.2 Microwave properties of sea ice

The SAR backscatter signature of sea ice depends both on SAR sensor parameters and on scattering characteristics of the illuminated area. The latter can be divided into *surface* and *volume scattering*. The relative contribution from the two scattering mechanisms depends on the *relative permittivity* (ϵ) of the sea ice, characterizing its electrical properties. It is denoted as

$$\epsilon = \epsilon' + j\epsilon'', \tag{3.1}$$

where the real component (ϵ') describes how easy an incident microwave passes through a dielectric interface, and the imaginary component (ϵ'') gives the electromagnetic loss of the material [Ulaby et al., 2014]. For sea ice, the relative permittivity mainly depends on microwave frequency, sea ice salinity and temperature. The relationship between ϵ' and $j\epsilon''$ controls the microwave *penetration depth* of sea ice, which hence decreases with increasing radar frequency, sea ice salinity and temperature. Due to its higher salinity, the relative permittivity of FYI is higher than of MYI, resulting in a larger fraction of surface scattering from FYI during winter conditions [Dierking, 2013; Hallikainen and Winebrenner, 1992]. Melt ponds have a considerably higher relative permittivity than both FYI and MYI, a characteristic which can possibly be used for melt pond investigations in SAR imagery [Scharien et al., 2012, 2014b]. This is further discussed in Paper III.

The strength of surface scattering is dependent on *surface roughness*, in addition to the relative permittivity of the media. The surface roughness of a scattering surface depends not only on the surface, but also on the properties of the transmitted wave. Hence, electromagnetic surface roughness is defined in relation to radar wavelength. A

common way to describe the roughness of a surface is the *root mean square height* (s_{rms}), defined as the standard deviation of the surface height variation. It can be written as

$$s_{rms} = \sqrt{\frac{1}{N}\sum_{i=1}^{N}(y_i - \overline{y})^2}, \tag{3.2}$$

where N represents the number of samples, $\overline{y}$ the mean height, and y_i the height of sample i [Leach, 2013]. The electromagnetic roughness accounts for the wavelength, and can be written ks_{rms}, where $k = \frac{2\pi}{\lambda}$ is the wave number of the incident wave. Surfaces that are very smooth compared to the wavelength will result in specular reflectance and appear very dark in SAR images (see Fig. 3.3). As s_{rms} increases, there will be an increased fraction of diffuse scattering from the surface, and for very rough surfaces, the backscatter is completely diffuse. The affect of surface roughness is also related to the SAR incidence angle. The angular dependency of surface roughness is strongest for smoothest surfaces (see Fig. 3.4). Defining a surface as smooth or rough is arbitrary. A common criterion for a smooth surface is the the Frauenhofer criterion, defined as

$$s_{rms} = \frac{\lambda}{32cos\theta}, \tag{3.3}$$

where θ is the incidence angle [Ulaby et al., 2014]. As surface scattering cannot be completely described analytically, models are often used to predict and interpret experimental data. The *Bragg scattering model*, or *small pertubation model* (SPM), is one of the most common models in radar remote sensing. The model is valid for surfaces filling the Bragg criterion, $ks_{rms} < 0.3$, corresponding to a root mean square height of 2.8 mm in C-band [Ulaby et al., 2014]. The influence of sea ice surface roughness on SAR signatures is further discussed in Paper II, where the effect of macro-scale surface roughness on summer sea ice signatures is evaluated.

Larger surface roughness structures, such as *ridges* and ice blocks, also affect the SAR signal from sea ice. They vary in size with heights from several centimeters to a few meters, and their influence on the SAR backscatter depends on their orientation with respect to the EM wave propagation, and internal structures in form of air bubbles and cracks. FYI ridges have steep slopes, high salinity, sharp corners, and air bubbles allowing for multiple scattering, and will produce bright signatures in SAR imagery. MYI ridges produces a less characteristic signature as they are more rounded, less steep-sided, and have fewer voids [Dierking, 2013; Ulaby et al., 2014].

Volume scattering occurs when a part of the incoming radar beam is transmitted into the sea ice volume and reflected back to the surface and the radar sight due to scattering processes within the sea ice. Structures interacting with the EM wave in the sea ice volume consist of gas bubbles, brine pockets, and crystal structures. The fraction, size, and shape of these inclusions will influence on the strength of the volume scattering, and these factors are dependent on the sea ice formation and growth history. Penetration depth will also control the efficiency of volume scattering, defining how large fraction

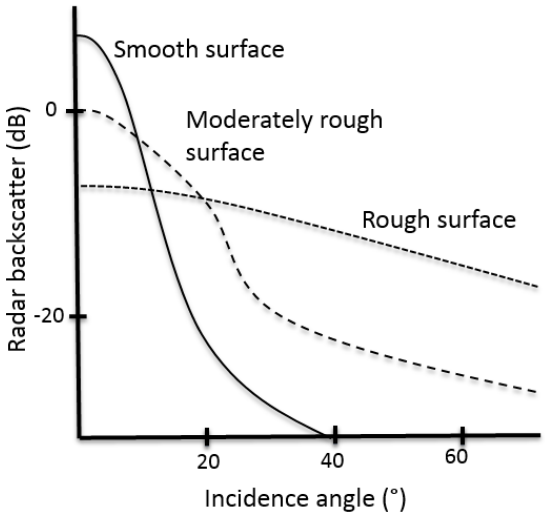

Figure 3.4: Microwave backscatter angular response for smooth, moderately rough and rough surfaces. Adapted from Ulaby et al. [1986].

of the sea ice volume that is seen by the radar. During winter, the low salinity of MYI allows for greater penetration into the sea ice volume than for FYI, and volume scattering is therefore more prominent for winter MYI [Dierking, 2013; Ulaby et al., 2014].

During summer, the microwave signature of sea ice changes dramatically. Wet snow on the sea ice surface suppresses volume scattering and could contribute a return signal of if its own [Dierking, 2013; Ulaby et al., 2014]. As the snow melts, superimposed sea ice resulting from melt and thaw cycles could roughen the sea ice surface, leading to increased backscatter [Hallikainen and Winebrenner, 1992]. The melt water of snow and ice contributes to the formation of melt ponds. Their influence on the sea ice SAR signature is dependent on their coverage, size distribution and wind conditions at the time of acquisition, parameters rapidly changing during the melt season [Scharien et al., 2012]. All these processes connected to melt, freezing and free water make microwave sea ice monitoring in the summer season extremely challenging. Chapter 4 gives a overview of summer sea ice studies with SAR.

3.3 SAR sensor parameters

SAR sensor parameters, such as frequency, polarisation, incidence angle, noise level and resolution, affect the SAR signature of sea ice, and strongly influence the results presented in Paper I-III. Specific applications introduce different restrictions on these parameters, and some examples of their influence on sea ice information gain are presented in the following.

Different frequencies are sensitive to sea ice properties of different kinds. The C-band

wavelength is comparable to the size of the scatterers within the ice volume, and has proven useful in distinguishing FYI and MYI during winter. X-band signatures are similar to those of C-band, but X-band measurements are more sensitive to small-scale surface roughness and sea ice inclusions. Deformed sea ice is easier to detect in L-band than at higher frequencies, and L-band allow for a larger penetration depth in the sea ice volume [Dierking, 2013; Onstott, 1992; Ulaby et al., 2014]. L-band has also a potential for sea ice type discrimination in the summer season [Casey et al., 2016]. Combinations of multiple frequencies can potentially increase the sea ice information gain by adding complementary information [Dierking, 2013; Kern et al., 2010].

The choice of polarimetric channels for sea ice monitoring also depends on the application. The co-polarisation channels (VV and HH) perform similarly for many sea ice types. However, the HH-channel gives a better discrimination between open water and sea ice during calm conditions, and is therefore often preferred by operational sea ice services. Depolarisations are captured by the cross-polarisation channels (HV and VH), and these can hence be used to separate deformed and level ice areas [Dierking, 2013; Onstott, 1992]. Combination of several polarimetric channels increases the amount of retrievable information.

SAR incidence angles from 20° to 50° are commonly used in sea ice investigations, and the preferred angle varies with application. For instance, discrimination between smooth and rough ice improves with increasing incidence angle, and ridges are easier identified at large incidence angles [Dierking, 2013; Onstott, 1992].

The SAR noise floor, or *noise equivalent sigma zero* (NESZ), determines the minimum detectable backscatter of a system. Different SAR systems have different NESZs. Very smooth ice can at some occasions fall below the noise floor. The cross-polarisation channels are most vulnerable, and the problem increases with increasing incidence angle [Dierking, 2013].

The SAR spatial resolution governs the size of sea ice structures possible to detect with SAR. Operational systems requires coverage of vast areas, and uses satellite SAR modes with large coverage and relative low resolution (~ 100 m). Higher resolution (~ 10 m) is needed to retrieve more detailed information about small-scale structures such as, e.g., surface roughness, ridges and melt ponds. Today, high resolution scenes have limited coverage and revisiting frequency, and is hence not utilized operationally.

Chapter 4

Summer sea ice studies with SAR

This thesis focuses on summer sea ice signatures in SAR imagery. Melt processes and rapid changes in sea ice microwave properties make summer sea ice investigations with SAR challenging. A brief review of studies involving summer sea ice studies with SAR is given in this chapter. The review is followed by an overview of selected polarimetric SAR features relevant for summer sea ice studies, with a focus on features utilized in Paper I-III. A description of the main method used to investigate statistical dependency between features and measured sea ice properties in this thesis is included at the end of the second section.

4.1 A brief review

Research on SAR and sea ice have been conducted for several decades, but the majority of the studies have focused on winter conditions [Onstott, 1992]. Early studies on SAR signatures of summer sea ice mainly focused on seasonal evolution, backscattering signatures, and scattering contrast between FYI and MYI [e.g. Barber et al., 1992; Carlström and Ulander, 1993; Carsey, 1985; Drinkwater and Argus, 1989; Gogineni et al., 1992; Holt and Digby, 1985; Livingstone et al., 1987; Onstott and Gogineni, 1985; Onstott et al., 1987; Winebrenner et al., 1994]. Seasonal evolution of backscatter intensities based on single-channel satellite SAR has also been investigated in more recent studies [De Abreu et al., 2001; Jeffries et al., 1997]. Detection of onset of melt with single-channel satellite SAR have been examined for individual years [Barber and Yackel, 1999; Kwok et al., 2003; Yackel et al., 2001] and inter-annually [Mahmud et al., 2016; Yackel et al., 2007]. Advancing to multi-polarimetric SAR, melt season sea ice polarimetric backscatter signatures have been explored with scatterometers for FYI [Scharien et al., 2010, 2012] and MYI [Isleifson et al., 2010], and the impact of macro-scale roughness on sea ice polarimetric SAR features during melt met attention in Fors et al. [2016b]. A number of studies have focused on sea ice classification and sea ice type discrimination in the summer season. Single-channel satellite SAR classification have proven difficult in C-band [Warner et al., 2013], while L-band results have been promising [Arkett et al., 2008;

Table 4.1: Literature survey of summer sea ice SAR studies.

Study	Area	Instrument	Frequency	Polarisation	Ice type	Focus
Onstott and Gogineni [1985]	CAA	Scatterometer (helicopter)	Ku, X, C, L	HH,HV,VV	FYI, MYI	SAR signatures
Onstott et al. [1987]	Fram Strait	Scatterometer (helicopter)	Ku, X, C, L	HH,HV,VV	FYI, MYI	SAR signatures
Livingstone et al. [1987]	CAA		Ku	HH,HV	FYI, MYI	Seasonal evolution
Holt and Digby [1985]	CAA	Seasat SAR, SAR (helicopter)	X, C, L	HH,HV	FYI	SAR signatures
Carsey [1985]	CAA	Seasat SAR	L	HH	FYI, MYI	Seasonal evolution
Drinkwater and Argus [1989]	Labrador Sea	Scatterometer (airborne)	C	HH	FYI	SAR signatures
Barber et al. [1992]	CAA	SAR (aircraft)	X	HH	FYI, MYI	Seasonal evolution
Gogineni et al. [1992]	Arctic	-	-	-	FYI, MYI	Review
Carlström and Ulander [1993]	Arctic Ocean	Scatterometer (ship)	C	Full	MYI	SAR signatures
Winebrenner et al. [1994]	Beaufort Sea	ERS-1	C	VV	MYI	Melt onset
Jeffries et al. [1997]	Beaufort Sea	ERS-1	C	VV	MYI	Seasonal evolution, melt ponds
Barber and Yackel [1999]	CAA	ERS-1	C	VV	FYI, MYI	Melt onset, surface albedo
Yackel and Barber [2000]	CAA	Radarsat-1	C	HH	FYI	Melt ponds
Hanesiak et al. [2001]	CAA	Radarsat-1	C	HH	FYI	Surface albedo
De Abreu et al. [2001]	CAA	Radarsat-1	C	HH	FYI	Sesonal evolution
Yackel et al. [2001]	Baffin Bay	Radarsat-1	C	HH	FYI	Melt onset
Kwok et al. [2003]	Arctic Ocean	Radarsat-1	C	HH	FYI, MYI	Melt onset
Scharien et al. [2007]	Hudson Bay	ENVISAT-ASAR	C	HH,VV	FYI	Surface albedo
Yackel et al. [2007]	Baffin Bay	Radarsat-1, ERS-1	C	HH,VV	FYI	Melt onset

Arkett et al. [2008]	CAA	Radarsat-1, ALOS/PALSAR	C, L	HH	FYI, MYI	Classification
Isleifson et al. [2010]	Beaufort Sea	Scatterometer (ship)	C	Full	MYI	SAR signatures
Kern et al. [2010]	Arctic Ocean	Scatterometer (helicopter)	S, C, X, Ku	Full	FYI	Classification, melt ponds
Scharien et al. [2010]	Beaufort Sea	Scatterometer (sled)	C	HH,VV	FYI	SAR signatures
Scharien et al. [2012]	Beaufort Sea, CAA	Scatterometer (sled)	C	Full	FYI	SAR signatures
Brath et al. [2013]	Arctic Ocean	Scatterometer (helicopter)	Ku, X, C, S	Full	FYI, MYI	Classification
Gill et al. [2013]	CAA	Radarsat-2	C	Full	FYI	Classification
Kim et al. [2013]	Chukchi Sea	TerraSAR-X	X	HH	MYI	Melt ponds
Warner et al. [2013]	Beaufort Sea	Radarsat-2	C	HH,HV	FYI, MYI	Classification
Mäkynen et al. [2014]	Arctic Ocean	ENVISAT-ASAR	C	HH	FYI, MYI	Melt ponds
Scharien et al. [2014b]	CAA	Scatterometer (sled)	C	HH,HV,VV	FYI	Melt ponds
Scharien et al. [2014a]	CAA	Radarsat-2	C	HH,VV	FYI	Melt ponds
Fors et al. [2015]	Fram Strait	Radarsat-2	C	HH,HV,VV	FYI, MYI	Melt ponds
Casey et al. [2016]	CAA	Radarsat-2, ALOS/PALSAR	C, L	HH,HV	FYI, MYI	Classification
Fors et al. [2016a]	Fram Strait	Radarsat-2, TerraSAR-X	X, C	Full	FYI, MYI	Segmentation
Fors et al. [2016b]	Fram Strait	Radarsat-2	C	Full	FYI, MYI	SAR signatures
Fors et al. [2016c]	Arctic Ocean	TerraSAR-X	X	HH,VV	FYI	Melt ponds
Han et al. [2016]	Chukchi Sea	TerraSAR-X	X	HH,VV	MYI	Melt ponds
Mahmud et al. [2016]	CAA	Radarsat-1, Radarsat-2	C	HH,	FYI, MYI	Melt onset

CAA denotes the Canadian Arctic Archipelago.

Casey et al., 2016]. Multi-polarimetric SAR features retrieved from satellite scenes have proven useful for sea ice discrimination both individually and combined [Fors et al., 2016a; Gill et al., 2013]. The combination of several frequencies was found to increase sea ice classification accuracy in Kern et al. [2010] and Brath et al. [2013]. Estimation of sea ice surface albedo and melt pond fraction from SAR during summer melt have also been explored. Single-polariation satellite SAR has proven useful in albedo estimations [Barber and Yackel, 1999; Hanesiak et al., 2001], while melt pond fraction estimations have showed varying results [Jeffries et al., 1997; Kim et al., 2013; Mäkynen et al., 2014; Yackel and Barber, 2000]. Using dual-polarisation SAR in estimation of albedo [Scharien et al., 2007] and melt pond fraction [Fors et al., 2015, 2016c; Han et al., 2016; Scharien et al., 2014a,b] improves the estimation results compared to use of single-polarisation. Combined use of different frequencies can also improve melt pond fraction estimation from SAR [Kern et al., 2010]. A survey of summer studies focusing on sea ice and SAR is presented in Table 4.1.

4.2 Polarimetric SAR features

Multi-polarimetric SAR satellites have introduced new opportunities in polarimetric characterisation of sea ice from space during the last two decades, also offering more advanced monitoring of summer sea ice. Polarimetric SAR features combine information from several polarimetric channels, and have a potential in describing various sea ice properties and scattering mechanisms. The following paragraphs give an introduction to the polarimetric SAR features employed in this thesis. Their relevance to sea ice studies in general are discussed, and any connection to summer sea ice investigations is highlighted. An overview of the presented features is given in Table 4.2, also indicating in which of this thesis' papers the features have been utilized.

Single-channel intensities

The backscatter intensities (σ^0) are single channel features, not utilizing multi-polarisation opportunities. They are found in the diagonal of the covariance matrix (Eq. 2.11), and are defined as

$$\sigma^0_{HH} = \langle |S_{HH}|^2 \rangle, \tag{4.1}$$
$$\sigma^0_{HV} = \langle |S_{HV}|^2 \rangle, \tag{4.2}$$
$$\sigma^0_{VH} = \langle |S_{VH}|^2 \rangle, \tag{4.3}$$
$$\sigma^0_{VV} = \langle |S_{VV}|^2 \rangle, \tag{4.4}$$

were $\langle |S_{XX}|^2 \rangle$ are $sigma^0$ calibrated. For many sea ice types, the co-polarisation intensities (σ^0_{HH} and σ^0_{VV}) behaves very similar. In winter, they can be used to discriminate, e.g., FYI and MYI, or sea ice and open water. σ^0_{HH} is often preferred for operational sea ice monitoring as it suppresses ocean clutter more than σ^0_{VV}, and hence is better suited for

Table 4.2: Overview of polarimetric SAR features investigated in this thesis.

Feature	**Paper(s)**
Features based on the covariance and coherency matrices	
Span ($SPAN$)	II
Geometric brightness (B)	I, II
Cross-polarisation ratio ($R_{VH/VV}$, $R_{HV/HH}$)	I, II
Co-polarisation ratio ($R_{VV/HH}$)	I, III
Co-polarisation correlation magnitude ($\|\rho\|$)	I, II, III
Co-polarisation correlation angle ($\angle\rho$)	I, II, III
Circular co-polarisation coefficient (ρ_{RRLL})	II
Degree of polarisation (DoP)	II
Features from polarimetric decompositions	
Freeman-Durden, surface scattering component (P_S))	II
Freeman-Durden, volume scattering component (P_V))	II
Eigenvalue-based features	
Entropy (H)	II, III
Anisotropy (A)	II
Alpha angle of the largest eigenvalue (α'_1)	II, III
Pedestal height (PH)	II
Statistical features	
Relative kurtosis (RK)	I, II, III

ice-water discrimination. The cross-polarisation intensities (σ^0_{HV} and σ^0_{VH}) are sensitive to sea ice surface roughness and volume scattering, as these processes depolarize the radar signal [Dierking, 2013; Onstott, 1992]. The co-polarisation intensities have been used to estimate onset of melt [e.g., Mahmud et al., 2016; Yackel et al., 2007]. After melt onset, the discrimination abilities of the backscatter intensities reduce due to wet snow and ice surfaces and freeze and thaw cycles, and different sea ice types' intensity signatures varies within hours and days [Gogineni et al., 1992].

Multi-channel intensities

Span ($SPAN$) and geometric brighness (GB) represent the total power of the scattering field, and are given as

$$SPAN = \mathrm{Tr}\{\mathbf{C}\}, \tag{4.5}$$

and

$$B = \sqrt[d]{det(\mathbf{C})}, \tag{4.6}$$

where d represent the number of polarimetric channels. Both represent the eigenvalues of the covariance matrix, but B is more sensitive to the smaller eigenvalues than $SPAN$. The multi-channel intensities increase with increasing surface roughness in snow-covered FYI [Gill and Yackel, 2012; Hossain et al., 2014; Moen et al., 2013], and $SPAN$ has proven

useful in discriminating FYI from other sea ice types during spring [Gill et al., 2013]. As the ice becomes rounded with age, the relationship to surface roughness is expected to weaken [Onstott, 1992; Ulaby et al., 2014].

Cross-polarisation ratio

Cross-polarisation ratio ($R_{VH/VV}$ or $R_{HV/HH}$) is defined as

$$R_{VH/VV} = \frac{\langle S_{VH} S_{VH}^* \rangle}{\langle |S_{VV}|^2 \rangle}, \tag{4.7}$$

or

$$R_{HV/HH} = \frac{\langle S_{HV} S_{HV}^* \rangle}{\langle |S_{HH}|^2 \rangle}, \tag{4.8}$$

and gives an estimate of the degree of depolarisation of the SAR signal [Drinkwater et al., 1992]. The ratio is hence expected to be sensitive to sea ice surface roughness and volume scattering. Increased discrimination between FYI and MYI, improved iceberg detection, and better ice-water separation is achieved by combining cross and co-polarisation channels in operational sea ice monitoring [Scheuchl et al., 2004].

Co-polarisation ratio

Co-polarisation ratio ($R_{VV/HH}$) is written as

$$R_{VV/HH} = \frac{\langle |S_{VV}|^2 \rangle}{\langle |S_{HH}|^2 \rangle}. \tag{4.9}$$

For smooth surfaces fulfilling the Bragg criterion ($ks < 0.3$), $R_{VV/HH}$ depends only on the sea ice complex permittivity and the local incidence angle, and is hence independent of surface roughness [Hajnsek et al., 2003]. For rougher surfaces, the ratio is expected to increase with incidence angle and relative permittivity, and decrease with increasing surface roughness [Drinkwater et al., 1991; Fung, 1994]. $R_{VV/HH}$ tends toward unity when volume scattering occurs [Scharien et al., 2012]. The feature has been used for melt pond fraction estimation in C-band, utilizing the different complex permittivity of melt ponds and sea ice [Fors et al., 2015; Scharien et al., 2012, 2014a,b].

Co-polarisation correlation coefficient

The co-polarisation correlation coefficient (ρ) is defined as

$$\rho = \frac{\langle S_{HH} S_{VV}^* \rangle}{\sqrt{\langle |S_{HH}|^2 \rangle \langle |S_{VV}|^2 \rangle}}, \tag{4.10}$$

and describes the degree of correlation between the co-polarisation channels [Drinkwater et al., 1992]. Both its magnitude ($|\rho|$) and phase ($\angle\rho$) have been utilized in sea ice studies.

For fully polarized backscattering, the returns from the HH and VV channels are perfectly correlated, and $|\rho|$ is unity. Depolarisation of the signal will reduce $|\rho|$ [Drinkwater et al., 1992]. Isleifson et al. [2010] found $|\rho|$ to vary with thickness of newly formed sea ice, and Han et al. [2016] related it to melt pond fraction.

$\angle\rho$ is often termed co-polarisation phase difference. As the relative phase of the co-polarisation waves changes in every scattering event, the mean and probability density distribution (PDF) of $\angle\rho$ are related to the scattering history [Drinkwater et al., 1992]. In the case of full correlation between the HH and VV channels, the probability density distribution of $\angle\rho$ tends towards a Dirac delta function. Han et al. [2016] found $\angle\rho$ to give useful information in melt pond fraction retrieval, and its distribution has been related to sea ice surface roughness in several springtime studies [Brekke et al., 2015; Gill and Yackel, 2012; Hossain et al., 2014].

Circular co-polarisation coefficient

Circular co-polarisation coefficient (ρ_{RRLL}) is defined as

$$\rho_{RRLL} = \frac{\langle|S_{HH} - S_{VV}|^2\rangle - 4\langle|S_{HV}|^2\rangle}{\langle|S_{HH} - S_{VV}|^2\rangle + 4\langle|S_{HV}|^2\rangle}, \tag{4.11}$$

and its elements can be retrieved from the coherency matrix (eq. 2.12). The feature is independent of relative permittivity for smooth surfaces ($ks < 1$), and is therefore sensitive to small-scale surface roughness [Hajnsek et al., 2003; Mattia et al., 1997; Schuler et al., 2002]. ρ_{RRLL} has been related to sea ice surface roughness during winter [Gupta et al., 2014; Wakabayashi et al., 2004], but has met little attention in SAR summer sea ice studies.

Degree of polarisation

Degree of polarisation (DoP) is a measure of coherence between the HH and VV channels. A DoP of one represents the fully polarized case, while complete depolarisation results in a zero value DoP [Lee and Pottier, 2009]. The feature is expressed in terms of the Stokes parameters (q_0, q_1, q_2 and q_3) [Raney, 2007]

$$DoP = \frac{\sqrt{q_1^2 + q_2^2 + q_3^2}}{q_0}. \tag{4.12}$$

This follows from the fundamental expression derived from the coherency matrix in Wolf [1959]. Hence, the Stokes parameters for the received signal in a backward scattering alignment (BSA) circular transmit/linear receive compact system can be written as [Cloude et al., 2012]

$$\begin{bmatrix} q_0 \\ q_1 \\ q_2 \\ q_3 \end{bmatrix} = \begin{bmatrix} \frac{1}{2}(t_{11} + t_{22} + t_{33} - \Im(t_{23})) \\ \Re(t_{12}) - \Im(t_{13}) \\ \Re(t_{13}) + \Im(t_{12}) \\ \Im(t_{23}) - \frac{1}{2}(t_{22} + t_{33} - t_{11}), \end{bmatrix} \tag{4.13}$$

were t_{xx} represents a complex element of the coherency matrix

$$\boldsymbol{T} = \frac{1}{2}\begin{bmatrix} t_{11} & t_{12} & t_{13} \\ t_{21} & t_{22} & t_{23} \\ t_{31} & t_{32} & t_{33} \end{bmatrix}. \tag{4.14}$$

Few sea ice studies have utilized DoP. Brekke et al. [2015] related it to sea ice surface roughness during springtime, while Espeseth et al. [2016] used it for reconstruction of quad-polarimetric data from hybrid polarity mode for sea ice.

The Freeman-Durden decomposition

The Freeman-Durden decomposition is a theoretical decomposition separating the scattering signal into three scattering mechanism; surface scattering (P_S), double-bounce scattering (P_D) and volume scattering (P_V). The sum of the three components equals the span. A full description of the decomposition method is given in Freeman and Durden [1998]. The method was first developed for forested regions, but has been widely used in other fields. P_S and P_V have been used to estimate contributions from surface and volume scattering in sea ice SAR scenes in several studies, and have also proven useful in sea ice segmentations [e.g. Casey et al., 2014; Gill and Yackel, 2012; Hossain et al., 2014; Komarov et al., 2015; Nakamura et al., 2005; Scheuchl et al., 2002a]. P_D is in general expected to be small or absent from sea ice backscatter [Hossain et al., 2014; Scheuchl et al., 2005]. Few SAR summer sea ice studies have employed the Freeman-Durden decomposition, but Gill et al. [2013] found P_V suitable for sea ice type discrimination of springtime FYI.

The $H/A/\alpha$ decomposition

The $H/A/\alpha$ decomposition is a polarimetric decomposition based on the eigenvalues and eigenvectors of the coherency matrix [Cloude and Pottier, 1997]. It consists of three components; the entropy (H), the anisotropy (A) and the mean scattering angle ($\bar{\alpha}$). The combination of them describes the scattering processes taking place at a given target. The decomposition has been employed for sea ice classification and iceberg detection in several studies [e.g., Dierking and Wesche, 2014; Gill et al., 2013; Hudier and Tolzczuk-Leclerc, 2013; Scheuchl et al., 2002b]. Parts of the decomposition were found to have potential in melt pond fraction estimation in Han et al. [2016].

H is a measure of the randomness of the scattering processes, and is defined as

$$H = -\sum_{i=1}^{d} p_i \log_d p_i, \tag{4.15}$$

where p_i is the relative magnitude of each eigenvalue,

$$p_i = \frac{\lambda_i}{\sum_{k=1}^{d} \lambda_k}, \tag{4.16}$$

and λ_i is the i^{th} eigenvalue of the coherency matrix ($\lambda_1 > \lambda_2 > \lambda_3$) [Cloude and Pottier, 1997]. $H = 0$ indicates a single dominant scattering mechanism, while $H = 1$ indicates totally depolarized backscatter. The original version of the decomposition included three polarmetric channels ($d = 3$). It can however also be utilized for dual-polarimetric SAR ($d = 2$) [Cloude, 2007; Skrunes et al., 2014], in this thesis marked with a apostrophe (H').

A describes the relative importance of the secondary scattering mechanisms, and is written as [Cloude and Pottier, 1997]

$$A = \frac{\lambda_2 - \lambda_3}{\lambda_2 + \lambda_3} \tag{4.17}$$

A is zero if the secondary scattering processes are equally strong, and higher values of A indicate dominance of one strong secondary scattering mechanism. For smooth surfaces, A has been suggested independent of dielectric properties, and hence sensitive to surface roughness [Hajnsek et al., 2003].

$\bar{\alpha}$ indicates the type of the mean scattering mechanism. It is defined as [Cloude and Pottier, 1997]

$$\bar{\alpha} = \sum_{i=1}^{d} p_i \alpha_i, \tag{4.18}$$

where α_i is the alpha angle of the i^{th} eigenvector $\mathbf{e}_i$

$$\alpha = cos^{-1}(|\mathbf{e}_i(1)|). \tag{4.19}$$

$\bar{\alpha}$ takes values between $0°$ and $90°$. Small values of $\bar{\alpha}$ suggest surface scattering, values around $45°$ indicate volume scattering, and higher values represent double-bounce scattering [Cloude and Pottier, 1997]. In the case of dual-polarisation, only two α_i angles can be retrieved, resulting in $\alpha'_1 + \alpha'_2 = 90$. It is then more useful to look at the angle of the dominant scattering mechanism, α'_1, than the mean of the two. $\bar{\alpha}$ have not been utilized in the work with these thesis, while α'_1 is explored in Paper III.

Pedestal height

Pedestal height (PH) is a measure of the presence of unpolarised scattering components in the average returned signal [Evans et al., 1988]. It is given as

$$PH = \frac{min(\lambda_1, \lambda_2, \lambda_3)}{max(\lambda_1, \lambda_2, \lambda_3)}. \tag{4.20}$$

PH is suggested to increase with increasing sea ice surface roughness for FYI during winter and spring [Hossain et al., 2014; Moen, 2014], but has not been investigated in summer sea ice studies.

Relative kurtosis

Relative kurtosis (RK) is a statistical SAR feature, which describes the shape of the distribution of scattering coefficients in SAR scenes. It is defined as Mardia's multivariate kurtosis of a sample, divided by the expected multivariate kurtosis of a complex normal distribution [Doulgeris and Eltoft, 2010; Mardia, 1970]

$$\mathrm{RK} = \frac{1}{L}\frac{1}{d(d+1)}\sum_{i=1}^{L}\left[\mathbf{s}_i^{*\dagger}\mathbf{C}^{-1}\mathbf{s}_i\right]^2. \tag{4.21}$$

RK is expected to separate deformed sea ice from level ice, due to differences in scattering coefficient distribution [Moen et al., 2013]. It is also expected to be sensitive to mixtures of surfaces, and was found related to melt pond fraction in Fors et al. [2015].

4.2.1 Statistical dependency

Several methods can be used to investigate statistical dependency between different parameters. In this thesis, Spearman's rank correlation coefficient (r) has been used to examine the statistical dependency between polarimetric SAR features and sea ice properties. The coefficient was chosen as it is a non-parametric measure of dependency, and is less sensitive to outliers than Pearson's linear correlation coefficient. It makes the assumption of a monotonic relationship. For a sample of size n, Spearman's rank correlation coefficient is defined as

$$r = 1 - \frac{6\sum d_i^2}{n(n^2-1)}, \tag{4.22}$$

where d_i is the difference in paired rank number i [Corder and Foreman, 2009]. Rank ties are assigned a rank equal to the average of their position in the ascending order of the values. The coefficient takes values between -1 and 1, where values of ± 1 corresponds to full correlation, while 0 corresponds to no correlation. A negative sign indicates an inverse relationship.

Spearman's rank correlation coefficient is utilized in the investigation of surface roughness SAR signature in Paper II, and in the study of melt ponds influence on the microwave signal in Paper III.

Chapter 5

Study areas and data sets

The work of this thesis is based on data acquired in the Arctic during two different campaigns organized by the Norwegian Polar Institute (NPI). The first campaign took place on fast-ice in the Fram Strait during August/September 2011, and form the basis for Paper I and II. The second campaign was located in an area of drift ice north of Svalbard in July/August 2012 and form the basis for Paper III. The research vessel R/V Lance was the main base of both campaigns. This chapter describes the study regions, and the data collected during the campaigns.

5.1 Fram Strait 2011

A coordinated collection of SAR satellite scenes and helicopter-borne measurements was performed in the western Fram Strait as a part of NPI's Fram Strait campaign 2011 (see Fig. 5.1). Fram Strait is a dynamic region characterized by the outflow of sea ice from the central Arctic Ocean [e.g., Kwok, 2009; Renner et al., 2014]. The sea ice cover is therefore a mix of FYI and MYI, with a large fraction of deformed sea ice [Renner et al., 2013a]. Southwards drift leads to fast movement of the sea ice in most of the Fram Strait, but a region with iceberg-fast ice forms in some years in western Fram Strait [Hughes et al., 2011]. This was the situation in 2011, and five high resolution X and C-band SAR satellite scenes were captured in this region during the campaign. In addition, airborne measurements of sea ice thickness and surface roughness were collected during a helicopter flight crossing the area. Downward-looking photos mapping the sea ice surface was also captured during the flight. The study region consisted of snow-free ponded FYI and MYI in different stages of development. Both level and deformed sea ice were represented in the scenes. The melt ponds had partly started to refreeze, but the fraction of refrozen melt ponds at the site is unknown as no ground-based measurements could be preformed at the site of the scenes. The unknown state of the melt ponds restricted the use of this data set for melt pond studies.

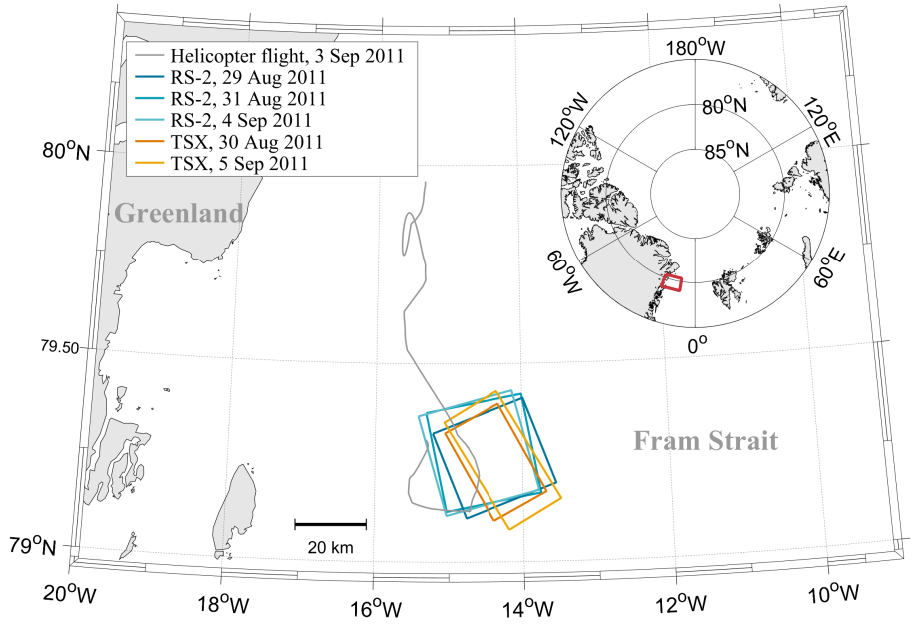

Figure 5.1: Map of the study area of Fram Strait 2011, showing the location of the satellite scenes and the track of the helicopter flight. The red box in the inset map displays the geographical position of the area shown.

5.2 ICE 2012

The ICE2012 campaign took place on drifting FYI north of Svalbard, in the southwestern Nansen Basin (see Fig. 5.2). The sea ice cover in the area generally consists of first or second-year ice [Moen et al., 2013; Renner et al., 2013b]. The surface roughness in the region is relatively low, due to little deformation and dominance of young ice [Beckers et al., 2015]. At the time of the campaign, the area consisted of very close drift ice. The sea ice was predominantly snow-free level ice in the late stages of melt, covered by saline melt ponds connected in complex networks [Divine et al., 2015; Hudson et al., 2013]. Melt pond fraction and sea ice thickness were mapped during five helicopter flights in the study region, and several high resolution X-band SAR satellite scenes were acquired during the campaign.

5.3 Data material

The Fram Strait and ICE2012 campaigns combined collection of satellite scenes with helicopter-borne and ground-based measurements. The following subsections describe the data material collected during the campaigns.

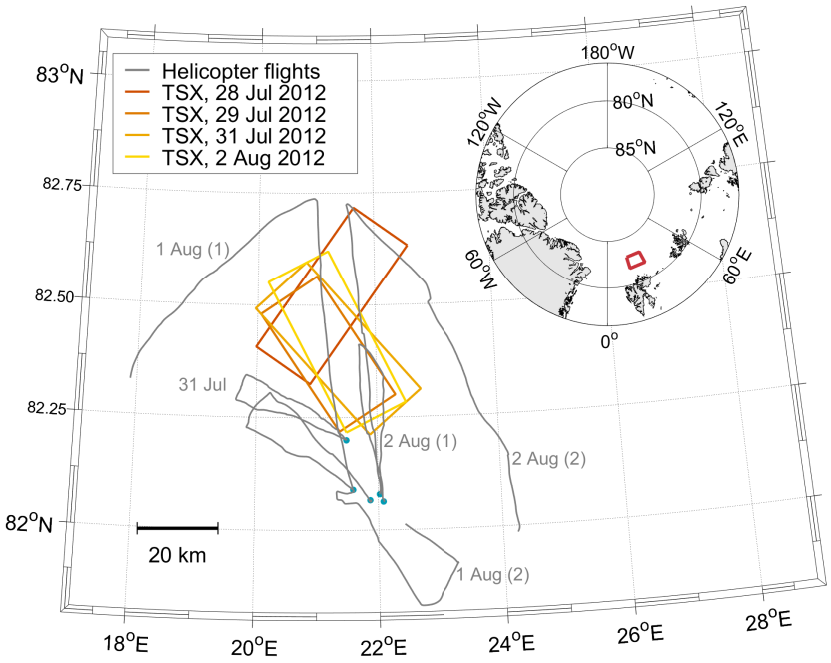

Figure 5.2: Map of the study area of ICE2012, showing the location of the satellite scenes employed in this thesis and the track of the helicopter flights. Blue dots mark the starting points of the flights. The red box in the inset map displays the geographical position of the area shown.

5.3.1 Satellite scenes

An overview of the satellite scenes employed in this thesis is presented in Table 5.1 and 5.2, and the position of the scenes are drawn in Fig. 5.1 and 5.2. The SAR scenes were acquired from two different satellites, covering X and C-band frequencies. C-band scenes were acquired from the Canadian Radarsat-2 during the Fram Strait campaign. The scenes were in standard Fine Quad-polarisation mode. X-band scenes from the German TerraSAR-X satellite were acquired both during the Fram Strait 2011 and the ICE2012 campaign. These scenes were all dual polarimetric StripMap scenes, with various polarisation combinations. Sensor properties of the satellites for the modes utilized in this thesis are given in Table 5.3.

5.3.2 Airborne and ground-based measurements

Numerous helicopter-borne and ground-based measurements were performed during the Fram Strait 2011 and ICE2012 campaigns. Only measurements utilized in this thesis are described in the following paragraphs.

Table 5.1: Overview of the Fram Strait 2011 data set. Date & time gives the start time, and CIA is the center incidence angle.

Date & time (UTC)	Sensor	Polarisation	CIA
29 Aug 2011 17:41	Radarsat-2	Quad	$38.2°$
30 Aug 2011 18:23	TerraSAR-X	Dual (HH,VV)	$29.4°$
31 Aug 2011 18:23	Radarsat-2	Quad	$48.2°$
3 Sep 2011 14:09	Helicopter fligth	–	–
4 Sep 2011 18:07	Radarsat-2	Quad	$44.4°$
5 Sep 2011 17:00	TerraSAR-X	Dual (VV,HV)	$25.9°$

Table 5.2: Overview of the part of the ICE2012 data set employed in this thesis. Date & time gives the start time, and CIA is the center incidence angle.

Date & time (UTC)	Sensor	Polarisation	CIA
28 Jul 2012 06:52	TerraSAR-X	Dual (HH,VV)	$36.9°$
29 Jul 2012 14:25	TerraSAR-X	Dual (HH,VV)	$37.9°$
31 Jul 2012 07:36	Helicopter flight	–	–
31 Jul 2012 13:51	TerraSAR-X	Dual (HH,VV)	$29.4°$
1 Aug 2012 07:22	Helicopter flight	–	–
1 Aug 2012 16:45	Helicopter flight	–	–
2 Aug 2012 11:21	Helicopter flight	–	–
2 Aug 2012 14:43	Helicopter flight	–	–
2 Aug 2012 14:51	TerraSAR-X	Dual (HH,VV)	$44.2°$

Table 5.3: Properties of the SAR sensors and modes used in this thesis [Airbus Defence and Space, 2014; MacDonald and Ltd, 2016]

	Radarsat-2	TerraSAR-X
Frequency	C-band (5.405 GHz)	X-band (9.65 GHz)
Mode	Fine Quad	StripMap
Incidence angle	$18° - 49°$	$20° - 45°$
Scene size	25 km $\times$ 25 km	15 km $\times$ 50 km
Resolution (slant rg. $\times$ az.)	5.2 m $\times$ 7.6 m	1.2 m $\times$ 6.6 m

Electromagnetic Induction Sounder

An electromagnetic induction sounder (EM-bird) was towed underneath the helicopter during the flights performed under Fram Strait 2011 and ICE2012, primarily measuring total snow plus sea ice thickness. There was very little snow on the sea ice surface during the campaings, hence the thickness measurements describe the sea ice thickness. The EM-bird utilizes the difference in conductivity between sea ice and water to find its height above the ice/water interface. This measure is combined with integrated laser altimeter measurements of the distance to the sea ice surface to retrieve the sea ice thickness. Flown at ~ 15 m height, the EM-bird has a footprint of about 50 m. The derived sea ice thickness has an accuracy of ± 0.1 m over level ice, but the thickness of ridges can be underestimated due to the large foot print [Haas et al., 2009; Renner et al., 2013a, 2014]. Figure 5.3 shows the EM-bird towed by the helicopter and displayed on the deck of R/V Lance.

Laser altimeter

In addition to retrieval of sea ice thickness, data from the laser altimeter integrated in the EM-bird can also be used to extract surface roughness [Beckers et al., 2015; von Saldern et al., 2006]. To achieve surface roughness, the helicopter altitude variations need to be removed from the data. This can be done by the three-step high and low-pass filtering method described by Hibler [1972]. The accuracy of the laser altimeter is about ± 15 mm. Several measures of surface roughness exists, in this thesis we focus on the root mean square height (s_{rms}) described in Section 3.2.

Stereo-camera system

Sea ice surface topography was investigated with a helicopter-borne stereo-camera system during ICE2012. The system consisted of two cameras, combined with global positioning system (GPS)/inertial navigation system (INS) and a laser altimeter mounted outside the helicopter. The camera shot overlapping photos, and these were used to construct a 2×2 cm digital terrain model (DTM) of the sea ice surface through photogrammetry. Surface roughness (s_{rms}) was estimated using random sampling to account for the spatial auto-correlation of the DTM, and had an accuracy of ± 4 cm according to *in situ* measurements from two test areas. A full description of the stereo-camera system setup is given in Divine et al. [2016].

Optical photos from the helicopter

Downward-looking photos were captured during the helicopter flights during the Fram Strait 2011 and ICE2012 campaigns. The photos gave good visual information about the sea ice surface. In addition, they were used to extract the surface fraction of sea ice, melt ponds and open water. In 2011, this was done by the method described in Renner

et al. [2013a], and in 2012 the method of Divine et al. [2015] was used. An example photo retrieved from the helicopter during ICE2012 is included in Fig. 5.3.

Meteorological measurements

Meteorological measurements of air temperature, surface air pressure and relative humidity were collected at a weather station onboard R/V Lance during the Fram Strait 2011 campaign. The height of the station was 40 m above sea level. The vessel was sailing during the campaign, and the measurements were performed within a distance of 150 km from the study site. To secure the validity of the meteorological measurements, they were compared to modeled data from the European Center for Medium-Range Weather Forecasts (ECMWF) [Dee et al., 2011], both at the position of R/V Lance and at the position of the satellite scenes.

During the ICE2012 campaign, an automatic weather station was located at the floe where R/V Lance was moored [Hudson et al., 2013]. Air temperature was measured with a temperature probe and wind speed was measured with a three-dimensional ultrasonic anemometer, both at an height of 2 m above the sea ice surface.

Sea ice cores

Ice cores were taken every other day during ICE2012. The cores described the sea ice type in the study region, and were used to extract temperature and salinity profiles of the sea ice.

5.4 Challenges and limitations

Working with data collection in the remote Arctic area will always be a challenge. Collecting SAR satellite data in combination with ground and helicopter-borne measurements requires thorough planning, close collaboration and a good portion of luck. Even if some planning is possible, factors like sea ice conditions, melt stage and meteorological situations will always introduce surprises. Acquiring satellite scenes with wanted specifications (polarisation, incidence angle etc.) might also be difficult with temporal and spatial restrictions. Despite difficulties and limitations in data collection, field data is crucial to develop a better understanding about the relation between SAR imagery and sea ice properties.

As R/V Lance is not an icebreaker, the position of the campaigns was not known exactly in advance. Even in the cases were ordered scenes and campaign area were co-located, weather partly prevented helicopter flights at the time of the acquisition of the scenes. Due to ice conditions, ground based observations and measurements were not possible to retrieve during Fram Strait 2011, restricting information about the state of melt ponds (open or refrozen) and sea ice morphology. During ICE2012, on-ice measurements were performed at the sea ice confined to the floe where R/V Lance was

moored. After data collection, co-location of EM-bird measurements, helicopter photos and sea ice has been challenging, both due to drift (ICE2012) and due to lacking GPS registration of the helicopter photos (Fram Strait 2011).

(a) Helicopter towing the EM-bird. Image courtesy of A. H. H. Renner.

(b) Downward-looking photo of ponded FYI (ICE2012).

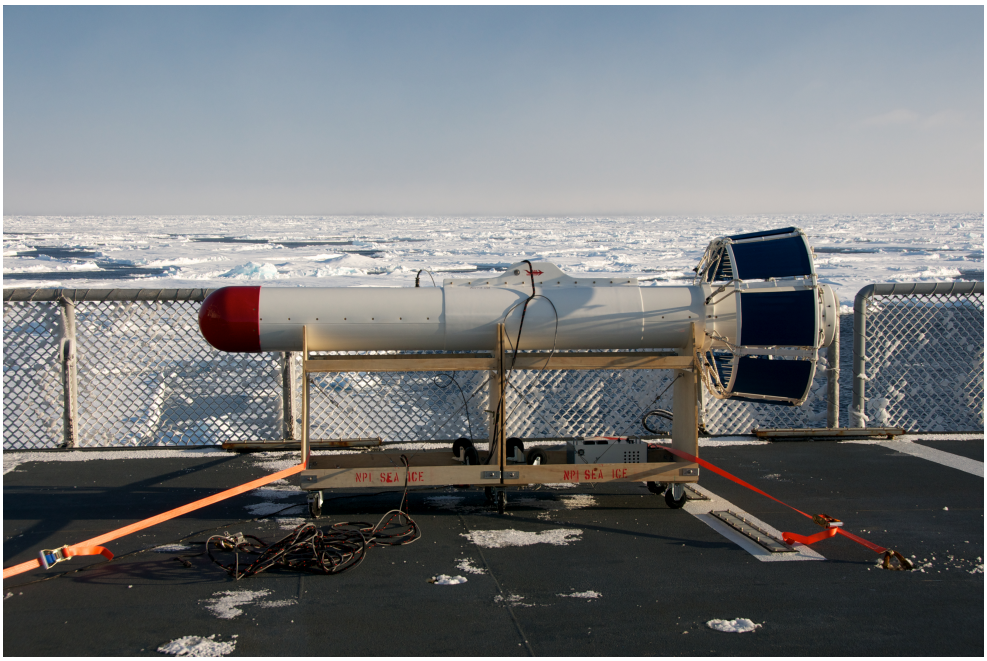

(c) The EM-bird. Image courtesy of A. H. H. Renner.

Figure 5.3: Illustrations of helicopter-borne measurements.

Chapter 6

Overview of Publications

This chapter gives a summary of the three papers presented in chapter 7- 9, and an overview of other scientific contributions.

6.1 Paper summaries

Paper I

Fors, A. S., Brekke, C., Doulgeris, A. P., Eltoft, T., Renner, A. H. H. and Gerland, S. **"Late-summer sea ice segmentation with multi-polarisation SAR features in C and X band"**, *The Cryosphere*, **10**(1): 401-415, February 2016.

Robust SAR sea ice segmentation is a challenge, and operational sea ice charts are mainly manually produced at present. Segmentation during melt conditions is especially demanding, and has met little attention in literature. Paper I investigates the potential of automatic sea ice segmentation by C and X-band multi-polarisation SAR during late summer. The study utilizes a feature-based mixture-of-Gaussian segmentation algorithm, employing six polarimetric SAR features describing different properties of sea ice backscatter. The algorithm has previously proven useful for segmentation of winter sea ice SAR scenes at C-band. Three quad-polarimetric Radarsat-2 scenes and two dual-polarimetric TerraSAR-X scenes acquired during the Fram Strait 2011 campaign are analysed in the study. Five different sea ice types, consisting of FYI and MYI in different stages of development, were identified in the area covered by the scenes. The sea ice type identification was based on sea ice thickness, surface roughness, and aerial photographs collected during a helicopter flight at the site.

The discrimination capacity of the individual polarimetric SAR features are evaluated through their ability to separate the different sea ice types. This is done by employing a maximum a posteriori (MAP) supervised classifier to test their individual discrimination skills, and by a qualitative study of their temporal consistency during changing meteorological conditions. All the individual features show potential in discriminating some of

the sea ice types from each other, both at C and X-band, but none of the features could efficiently separate the total set of sea ice types. This suggests that a combination of the features has potential for an improved sea ice segmentation. *Co-polarisation ratio* and *co-polarisation correlation magnitude* produce temporally inconsistent discrimination results, while *relative kurtosis*, *geometric brightness*, *cross-polarisation ratio* and *co-polarisation correlation angle* show good temporal consistency during changing temperature conditions. The latter four features are suggested to form a reduced feature-set, possibly improving the temporal consistency of a sea ice summer segmentation. The segmentation algorithm is tested with both the full and the reduced feature-set. In C-band, the segmentation algorithm displays a good ability of discriminating the identified sea ice types, and shows high temporal consistency. The results in X-band are poorer, only some of the sea ice types are discriminated in one of the two scenes. Reducing the feature-set improves the result for the poorest segmented X-band scene. The lower X-band performance is not necessarily a result of higher frequency, but might also relate to fewer polarisation channels, lower incidence angles, and difficult geophysical conditions at the time of the acquisitions.

Paper I adds knowledge to how the choice of polarimetric SAR features influences the information gain from SAR imagery, and highlights the sea ice segmentation capability of both C- and X band during late summer. Segmentation of sea ice SAR scenes is a first step towards sea ice classification; not only separating but also labeling different sea ice types. An improved understanding of the SAR signature of various geophysical sea ice properties is needed to expand from sea ice segmentation to classification. Paper II and III investigate how two important summer sea ice properties (surface roughness and melt pond fraction) influence polarimetric SAR imagery.

Paper II

Fors, A. S., Brekke, C., Gerland, S., Doulgeris, A. P. and Beckers, J. F. **"Late Summer Arctic Sea Ice Surface Roughness Signatures in C-Band SAR Data"**, *IEEE Journal of Selected Topics in Applied Earth Observation and Remote Sensing*, **9**(3): 1199-1215, March 2016.

Sea ice surface roughness strongly influences the polarimetric SAR signature of sea ice. During summer melt, surface scattering is expected to dominate the sea ice backscatter, enhancing the importance of surface roughness. Paper II investigates the influence of macro-scale sea ice surface roughness on C-band polarimetric SAR features in the late summer season. Three quad-polarimetric Radarsat-2 scenes acquired during the Fram Strait 2011 campaign are compared with sea ice surface roughness estimated from laser altimeter measurements collected during a helicopter flight crossing the area covered by the scenes. Root mean square height is used to describe sea ice surface roughness in the study.

Nine out of the fourteen investigated polarimetric SAR features are found correlated

to sea ice surface roughness with a Spearman's correlation coefficient better than ± 0.6 in at least one of the SAR scenes included in the study. The results vary from scene to scene, and only six features display a strong correlation to surface roughness in more than one scene. The between-scene variation is explained by different scene incidence angles and changes in meteorological conditions and micro-scale surface roughness during the campaign. *Circular co-polarisation coefficient* is suggested to be the best all-round polarimetric feature, due to a temporally stable performance and comparable numerical values in the three investigated satellite scenes.

The study shows that direct interpretation of macro-scale surface roughness from individual SAR features is challenging during summer season, but also highlights that knowledge of temperature and weather history could largely improve the quality of the interpretation. The results of the study deviate from findings in previous studies on snow-covered FYI in winter and spring, demonstrating that macro-scale sea ice surface roughness signatures in SAR imagery change with season and sea ice type.

Paper III

Fors, A. S., Divine, D. V., Doulgeris, A. P., Renner, A. H. H. and Gerland S. **"Signature of Arctic first-year ice melt pond fraction in X-band SAR imagery"**, *The Cryosphere*, submitted, May 2016, published in *The Cryosphere Discuss.* August 2016, revised November 2016.

The fractional coverage of melt ponds on Arctic sea ice varies rapidly during the melt season, and their presence and properties change the polarimetric SAR signature of the sea ice. In paper III, the influence of melt pond fraction on different polarimetric X-band SAR features is exploited. The data set collected during the ICE2012 campaign allows for investigations of well-documented and open melt ponds on drifting FYI, and is therefore utilized in the study. From the data set, melt pond fractions retrieved from down-looking images captured with a helicopter-borne camera system are combined with four dual-polarimetric TerraSAR-X scenes. Meteorological data and ice core moorings are also employed.

The study reveals statistically significant relationships between several of the investigated polarimetric SAR features and the mapped melt pond fraction. The relations are strongly dependent on wind speed. At intermediate wind speeds, *co-polarisation ratio* is the most promising feature for melt pond fraction estimation. At low wind speeds, the relationship disappears, and *VV intensity* becomes the preferred feature. In addition to wind speed dependence, the results are also sensitive to changes in SAR incidence angle. Based on the results, two regression fits for melt pond fraction estimation are suggested, reflecting the two different wind speed regimes. The fits are qualitatively evaluated both locally and for the full satellite scenes included in the study. On a local scale, the correlations are found weak, but at a full scene scale they manage to produce melt pond fraction estimates deviating with less than 4% from the mapped fraction in

the study region. The effect of system noise is also highlighted in the study, as 25% of the backscatter signal is found to be below the noise floor at an incidence angle of $44°$. The low signal-to-noise ratio is restricting the use of polarimetric SAR features at high incidence angles.

Paper III highlights that melt ponds make a significant signature on several polarimetric features in X-band SAR imagery, and that X-band SAR in the future could have a potential for retrieval of melt pond fraction. Compared to C-band SAR studies, the use of X-band SAR in melt pond fraction estimation is slightly more restricted due to limitations concerning wind speeds. The low noise floor of TerraSAR-X is also restricting the usable range of incidence angles. Despite this, the findings could open for prospective improved and extended monitoring of melt ponds from space.

6.2 Other publications and presentations

As first author

1. Fors, A. S., Brekke, C., Gerland, S., Doulgeris, A. P. and Eltoft, T. "Extraction of late summer sea ice properties from polarimetric SAR features in C- and X-band". In*Proc. POLinSAR 2015*. European Space Agency (ESA SP-729), Frascati, Italy, 25-30 January, 2015.

2. Fors, A. S., Doulgeris, A. P., Renner, A. H. H., Brekke, C. and Gerland, S. "On the relation between polarimetric sythetic aperture radar (SAR) features and sea ice melt pond fraction". In *2015 IEEE Geocience and Remote Sensing Symposium (IGARSS)*, pp. 3428-3431, Milano, Italy, 26-31 July, 2015.

As co-author

1. Gerland, S., Brandt, O., Hansen, E., Renner, A. H. H., Granskog, M. A., Forsström, S., Eltoft, T., Fors, A. F., Moen, M.-A., Doulgeris, A. P., Beckers, J. F. and Hughes, N. "Satellite calibration and validation experiments over Arctic sea ice in the vicinity of Svalbard". In *CryoSat validation workshop 2011*. European Space Agency (ESA SP-717), Frascati, Italia, 1-4 February, 2011.

2. Eltoft, T., Fors, A. S., Moen, M.-A, Renner, A. H. H., Doulgeris, A. P., Gerland. S. and Ferro-Famil, L. "A multi-polarization study of Arctic sea ice in C-band and X-band". In *Proc. SEASAR 2012*. European Space Agency (ESA SP-709), Tromsø, Norway, 18-22 June, 2012.

3. Wang, C. Renner, A. H. H., Gerland, S., Anfinsen, S. N., Brandt, O., Doulgeris, A. P., Dumont, M., Eltoft, T., Fors, A. S., Granskog, M. A., Haapala, J., Helm, V., Hendricks, S., Hudson, S. R., Hughes, N., Lensu, M., Li, Z., Moen, M.-A., Sandven, S., Skourup,

H., Spreen, G. and Zygmuntowska M. "In-situ calibration and validation of CryoSat-2 observations over Arctic first year sea ice north of Svalbard". In *Earth Observation and Cryosphere Science*, Frascati, Italy, 13-16 November 2012, not published.

4. Gerland, S., Renner, A. H. H., Spreen, G., Divine, D. V., Granskog, M. A., Hansen, E., Hudson, S. R., Doulgeris, A. P., Fors, A. S., Moen, M.-A., Hughes, N. and Storvold, R. "Validation and complementing of SAR satellite surveys over Arctic Sea ice by multiple simultaneous sets of measurements". In *POAC'13: The international conferences on port and ocean engineering under Arctic conditions*, Espoo, Finland, 9-13 June, 2013.

5. Gerland, S., Spreen, G., Eltoft, T., Renner, A. H. H., Moen, M.-A., King, J., Granskog, M.A., Hughes, N., Fors, A. S. and Wagner, P. "Observation-based validation and calibration of sea ice satellite products and data". In *Proceedings of the 22nd IAHR International Symposium on Ice*, pp. 765-770, Singapore, 11-15 August, 2014.

6. Dierking, W., Zhang, X., Mäkynen, M., Similä, M., Karvonen, J., Tonboe, R., Pedersen, L. T., Hollands, T., Linow, S., Griebel, J., Berg, A., Eriksson, L., Saldo, R., Muckenhuber, S., Doulgeris, A. P, Lohse, J., Fors, A. S., Kræmer, T., Eltoft, T., Moen, M.-A., Hughes, N. and Wagner, P. "Selected European Studies On Sea Ice Classification And Drift Retrieval As Basis For Collaborative Projects During Dragon 4". In *The 2016 Dragon 3 Final Results & Dragon 4 KO Symposium*, Wuhan, China, 4-8 July, 2016, not published.

Chapter 7

Paper 1:
Late summer sea ice segmentation with multi-polarisation SAR features in C- and X-band

Ane S. Fors, Camilla Brekke, Anthony P. Doulgeris, Torbjørn Eltoft, Angelika H. H. Renner and Sebastian Gerland

Published in: *The Cryosphere*, **10**(1): 401-415, February 2016.

Chapter 8

Paper 2:
Late summer Arctic Sea Ice Surface Roughness Signatures in C-Band SAR Data

Ane S. Fors, Camilla Brekke, Sebastian Gerland, Anthony P. Doulgeris and Justin F. Beckers

Published in: *IEEE Journal of Selected Topics in Applied Earth Observation and Remote Sensing*, **9**(3): 1199-1215, March 2016.

Chapter 9

Paper 3:
Signature of Arctic first-year ice melt pond fraction in X-band SAR imagery

Ane S. Fors, Dmitry V. Divine, Anthony P. Doulgeris, Angelika H. H. Renner and Sebastian Gerland

In review: *The Cryosphere*, submitted 19 May 2016, published in *The Cryosphere Discuss.* August 2016, revised November 2016.

Chapter 10

Conclusions

The work presented in this thesis explores the potential of multi-polarisation satellite SAR for extraction of sea ice information during the summer season. Below follows a summary of our research conclusions, and a future outlook discussing remaining challenges in this field of research.

10.1 Research conclusions

In the work of this thesis, we started out with exploring the potential of feature-based segmentation of summer sea ice with X and C-band SAR. Paper I revealed that some polarimetric SAR features are more sensitive to changes in air temperature and sea ice morphology than others. The findings highlighted that choice of features is important for summer sea ice segmentation, and essential for interpretation of the segments. The study also showed that sea ice segmentation in summer SAR scenes is possible, despite challenges introduced by melt and changing meteorological conditions. In C-band, the feature-based segmentation algorithm produced a temporally consistent sea ice segmentation. The X-band results were slightly poorer, possibly explained by fewer available polarisation-channels, lower SAR incidence angles and higher SAR frequency. To advance from segmentation to classification, or labeling the segments, an improved understanding of the influence of different sea ice properties on polarimetric SAR features was found necessary. In the summer season, surface roughness and presence of melt ponds are important properties influencing sea ice SAR imagery, and these were brought into focus in the following work.

The influence of macro-scale surface roughness on different C-band polarimetric SAR features was investigated in Paper II. The study showed significant relationships between several polarimetric features and sea ice surface roughness in individual SAR scenes. The relationships were however found to be temporally unstable, possibly due to different SAR incidence angles, and changes in meteorological conditions and micro-scale surface roughness during the week of study. Knowledge of weather history was found to improve the interpretation of the results. The findings in Paper II differ from

findings in other seasons, demonstrating the importance of season specific studies.

Paper III brings new insight to the influence of melt pond fraction on different polarimetric SAR features, and the possibilities of melt pond fraction estimation from dual polarimetric X-band SAR. Several polarimetric features were found correlated with melt pond fraction in the study. Wind speed and incidence angle strongly influenced the result. Compared with results results from previous studies in C-band, the melt pond fraction estimation possibilities were found to be more limited in X-band, due to wind-speed restrictions related to surface roughness of the melt ponds. The high noise floor of TerraSAR-X was also restricting the use of high incidence angles. The relationships found between the polarimetric SAR features and observed melt pond fraction in Paper III were not strong enough to be used for operational modeling of melt pond fraction. However, the results display a future potential of melt pond fraction estimation from X-band SAR. Improved methods and more satellite data are required for future progress.

The results from Paper I-III reveal opportunities of sea ice information extraction from X and C band SAR during summer. They demonstrate the possibility of sea ice segmentation, and show how surface roughness and presence of melt ponds influence the signature of polarimetric SAR features during melt season. Knowledge about weather history and current meteorological conditions are found to be important for interpretation of the relation between polarimetric SAR features and sea ice properties in all three papers. This highlights that successful melt season investigations of sea ice with SAR is strongly dependent on accurate meteorological information.

10.2 Future outlook

The Arctic sea ice regime changes towards longer melt seasons and more seasonal sea ice. This implies an increased need of information about melt season sea ice. The work of this thesis explore the potential of using polarimetric satellite-borne SAR in melt season sea ice investigations, but together with other studies performed in the field, it only scratches the surface. More data and extensive studies are needed to develop robust methods for sea ice information retrieval from SAR during summer melt.

X and C-band frequencies have been utilized in this thesis, and have shown different qualities. Other studies have also found L-band frequency useful for summer sea ice investigations. Different frequencies might be used for different tasks, but could also provide complementary information when used together. More effort should be put into combined used of different frequencies in future studies.

Polarimetric features have formed the basis in our work. Full polarimetric satellite SAR scenes contain more information about sea ice properties than single-polarimetric scenes, but the swath width is too narrow for operational use. Recent and future SAR missions introducing compact polarimetry and full polarimetric scenes with wider swath width make studies on the polarimetric signatures of sea ice more important, and could open for improved sea ice information retrieval from satellite SAR on larger spatial scales

in the future. Continued efforts in exploring optimum channel-combinations for different sea ice applications are therefore needed.

Combined collection of field data and SAR scenes are crucial for improved understanding of the interaction between SAR backscatter and sea ice during all seasons, and have been a foundation pillar in the work of this thesis. The field data presented Paper I-III is a result of a close collaboration between the remote sensing and sea ice communities in Tromsø. Increased effort should be paid in international collaborations in coordinated field and remote sensing data collection. Increased accessibility to already existing data could also improve calibration and validation possibilities of sea ice SAR scenes. In the work of these thesis, meteorological information has proven to be a key factor in interpreting SAR scenes in the summer season. Access to meteorological measurements in the Arctic is sparse. Utilizing and extending the meteorological measurements performed by autonomous buoys can increase the accessible amount of meteorological data. Meteorological models should also be used to a larger extent in data fusion with satellite SAR sea ice scenes to increase the information gain in future studies.

To advance in use of SAR in sea ice classification and monitoring, an improved understanding of the interaction between microwave backscatter and sea ice geophysical properties is needed. For the summer season, the effect of changing temperature, desalination, freeze and melt processes, surface roughness and presence of melt ponds should be further studied. The impact of SAR incidence angle and resolution should also meet more focus. Combined efforts in theoretical, laboratory, and empirical studies are needed to progress in this field, both utilizing conventional 2-D SAR, and SAR tomography.

Finally, sea ice is not only sea ice. Its properties changes with location, formation, growth and melt processes. A large part of the studies performed on SAR and summer sea ice have been located on fast-ice. Fast-ice is comfortable to work on as it does not move, but it is not representative for the Arctic. Most of the study sights have also been located in the Canadian Arctic. A larger variety of sea ice types and study sites in SAR investigations should be aimed for in the future. With the recent regime changes towards a thinner and more mobile sea ice cover, more focus on drift-ice is especially important.

Bibliography

Airbus Defence and Space. "TerraSAR-X Image Product Guide". URL: http://www2.geo-airbusds.com/files/pmedia/public/r459_9_201408_tsxx-itd-ma-0009_tsx-productguide_i2.00.pdf, visited 4 April 2016, August 2014.

Arkett, M., Flett, D. G., De Abreu, R., Clemente-Colon, P., Woods, J. and Melchior, B. "Evaluating ALOS-PALSAR for Ice Monitoring - What Can L-band do for the North American Ice Service?" In *IGARSS 2008 - 2008 IEEE International Geoscience and Remote Sensing Symposium (Vol.5)*, pp. 188–191. Boston, MA, USA, 7-11 July, 2008.

Arkett, M., Braithwaite, L., Pestieau, P., Carrieres, T., Pogson, L., Fabi, C. and Geldsetzer, T. "Preparation by the Canadian Ice Service for the Operational Use of the RADARSAT Constellation Mission in Their Ice and Oil Spill Monitoring Programs". *Canadian Journal of Remote Sensing*, **41**(5): 380–389, September 2015.

Barber, D. G. and Yackel, J. J. "The physical, radiative and microwave scattering characteristics of melt ponds on Arctic landfast sea ice". *International Journal of Remote Sensing*, **20**(10): 2069–2090, January 1999.

Barber, D. G., Flett, D. G., De Abreu, R. A. and LeDrew, E. F. "Spatial and Temporal Variation of Sea Ice Geophysical Properties and Microwave Remote Sensing Observations: The SIMS'90 Experiment". *ARCTIC*, **45**(3), January 1992.

Beckers, J. F., Renner, A. H. H., Spreen, G., Gerland, S. and Haas, C. "Sea-ice surface roughness estimates from airborne laser scanner and laser altimeter observations in Fram Strait and north of Svalbard". *Annals of Glaciology*, **56**(69): 235–244, 2015.

Brath, M., Kern, S. and Stammer, D. "Sea Ice Classification During Freeze-Up Conditions With Multifrequency Scatterometer Data". *IEEE Transactions on geoscience and remote sensing*, **51**(6): 3336–3353, 2013.

Breivik, L., Carrieres, T., Eastwood, S., Fleming, A., Girard-Ardhuin, F., Karvonen, J., Kwok, R., Meier, W., Mäkynen, M., Pedersen, L., Sandven, S., Similä, M. and Tonboe, R. "Remote sensing of sea ice". In *Proceedings of OceanObs'09: Sustained Ocean Observations and Information for Society (Vol.2)*, edited by J. Hall, H. D. E. and D. Stammer. European Space agency (ESA WPP-306), Venice, 21-25 September, 2009.

Brekke, C., Grahn, J. and Doulgeris, A. P. "Quad-polarimetric SAR for roughness and deformation characterization of sea ice at Hopen". In *Proc. POLinSAR. 2015*. European Space agency (ESA SP-729), Frascati, Italy, 26-30 January, 2015.

Canada Centre for Mapping and Earth Observation. "Tutorial: Radar Polarimetry". URL: http://www.nrcan.gc.ca/earth-sciences/geomatics/satellite-imagery-air-photos/satellite-imagery-products/educational-resources/9275, visited 15 March 2016, November 2015.

Carlström, A. and Ulander, L. M. H. "C-band backscatter signatures of old sea ice in the central Arctic during freeze-up". *IEEE Transactions on Geoscience and Remote Sensing*, **31**(4): 819–829, July 1993.

Carsey, F. D. "Summer Arctic sea ice character from satellite microwave data". *Journal of Geophysical Research*, **90**(C3): 5015–5034, 1985.

Casey, J. A., Beckers, J. F., Busche, T. and Haas, C. "Towards the retrieval of multi-year sea ice thickness and deformation state from polarimetric C- and X-band SAR observations". In *2014 IEEE Geoscience and Remote Sensing Symposium*, pp. 1190–1193. IEEE, July 2014.

Casey, J. A., Howell, S. E. L., Tivy, A. and Haas, C. "Separability of sea ice types from wide swath C- and L-band synthetic aperture radar imagery acquired during the melt season". *Remote Sensing of Environment*, **174**: 314–328, March 2016.

Cloude, S. R. "The dual polarisation entropy/alpha decomposition: A PALSAR case study". In *Proc. POLinSAR 2007*. European Space Agency (ESA SP-644), Frascati, Italy, 22-26 January, 2007.

Cloude, S. R. and Pottier, E. "An entropy based classification scheme for land applications of polarimetric SAR". *IEEE Transactions on Geoscience and Remote Sensing*, **35**(1): 68–78, 1997.

Cloude, S. R., Goodenough, D. G. and Chen, H. "Compact Decomposition Theory". *IEEE Geoscience and Remote Sensing Letters*, **9**(1): 28–32, 2012.

Corder, G. W. and Foreman, D. I. *Nonparametric Statistics for Non-Statisticians: A Step-by-step approach*. John Wiley & Sons, Inc., Hoboken, NJ, USA, 2009.

De Abreu, R., Yackel, J. J., Barber, D. G. and Arkett, M. "Operational Satellite Sensing of Arctic First-Year Sea Ice Melt". *Canadian Journal of Remote Sensing*, **27**(5): 487–501, October 2001.

Dee, D. P., Uppala, S. M., Simmons, A. J., Berrisford, P., Poli, P., Kobayashi, S., Andrae, U., Balmaseda, M. A., Balsamo, G., Bauer, P., Bechtold, P., Beljaars, A. C. M., van de Berg, L., Bidlot, J., Bormann, N., Delsol, C., Dragani, R., Fuentes, M., Geer, A. J.,

Haimberger, L., Healy, S. B., Hersbach, H., Hólm, E. V., Isaksen, L., Kållberg, P., Köhler, M., Matricardi, M., Mcnally, A. P., Monge-Sanz, B. M., Morcrette, J. J., Park, B. K., Peubey, C., de Rosnay, P., Tavolato, C., Thépaut, J. N. and Vitart, F. "The ERA-Interim reanalysis: Configuration and performance of the data assimilation system". *Quarterly Journal of the Royal Meteorological Society*, **137**: 553–597, 2011.

Dierking, W. "Sea Ice Monitoring by Synthetic Aperture Radar". *Oceanography*, **26**(2): 100–111, June 2013.

Dierking, W. and Wesche, C. "C-Band Radar Polarimetry - Useful for Detection of Icebergs in Sea Ice?" *IEEE Transactions on Geoscience and Remote Sensing*, **52**(1): 25–37, January 2014.

Divine, D. V., Granskog, M. A., Hudson, S. R., Pedersen, C. A., Karlsen, T. I., Divina, S. A., Renner, A. H. H. and Gerland, S. "Regional melt-pond fraction and albedo of thin Arctic first-year drift ice in late summer". *Cryosphere*, **9**: 255–268, 2015.

Divine, D. V., Pedersen, C. A., Karlsen, T. I., Aas, H. F., Granskog, M. A., Hudson, S. R. and Gerland, S. "Photogrammetric retrevals and analysis of small scale sea ice topography during summer melt". *Cold Regions Science and Technology*, 2016. (in review).

Doulgeris, A. P. and Eltoft, T. "Scale Mixture of Gaussian Modelling of Polarimetric SAR Data". *EURASIP Journal on Advances in Signal Processing*, **2010**: 1–13, 2010.

Drinkwater, M., Kwok, R., Rignot, E., Israelsson, H., Onstott, R. G. and Winebrenner, D. P. "Potential Applications of Polarimetry to the Classification of Sea Ice". In *Microwave Remote Sensing of Sea Ice*, edited by F. D. Carsey, volume 68 of *Geophysical Monograph Series*, pp. 419–430. American Geophysical Union, Washington, DC, USA, 1992.

Drinkwater, M. R. and Argus, S. D. "LIMEX'87: international experiment in the Labrador Sea Marchginal ice zone". *Polar Record*, **25**(155): 335–342, October 1989.

Drinkwater, M. R., Kwok, R., Winebrenner, D. P. and Rignot, E. "Multifrequency polarimetric synthetic aperture radar observations of sea ice". *Journal of Geophysical Research*, **96**(C11): 20679–20698, 1991.

Eicken, H. "Ocean science: Arctic sea ice needs better forecasts". *Nature*, **469**(7450): 431–433, 2013.

Eicken, H., Grenfell, T. C., Perovich, D. K., Richter-Menge, J. and Frey, K. "Hydraulic controls of summer Arctic pack ice albedo". *Journal of Geophysical Research*, **109**(C8): C08007, 2004.

Espeseth, M. M., Brekke, C. and Anfinsen, S. N. "Hybrid-Polarity and Reconstruction Methods for Sea Ice With L- and C-Band SAR". *IEEE Geoscience and Remote Sensing Letters*, pp. 1–5, 2016.

Evans, D. L., Farr, T. G., van Zyl, J. J. and Zebker, H. A. "Radar polarimetry: analysis tools and applications". *Geoscience and Remote Sensing, IEEE Transactions on*, **26**(6): 774–789, 1988.

Fors, A. S., Doulgeris, A. P., Renner, A. H. H., Brekke, C. and Gerland, S. "On the releation between polarimetric synthetic aperture radar (SAR) features and sea ice melt pond fraction". In *2015 IEEE International Geoscience and Remote Sensing Symposium (IGARSS)*, pp. 3441–3445. Milano, Italy 26-31 July, 2015.

Fors, A. S., Brekke, C., Doulgeris, A. P., Eltoft, T., Renner, A. H. H. and Gerland, S. "Late-summer sea ice segmentation with multi-polarisation SAR features in C and X band". *The Cryosphere*, **10**(1): 401–415, February 2016a.

Fors, A. S., Brekke, C., Gerland, S., Doulgeris, A. P. and Beckers, J. F. "Late Summer Arctic Sea Ice Surface Roughness Signatures in C-Band SAR Data". *IEEE Journal of Selected Topics in Applied Earth Observations and Remote Sensing*, **9**(3): 1199–1215, March 2016b.

Fors, A. S., Doulgeris, A. P., Divine, D. V., Renner, A. H. and Gerland, S. "Signature of Arctic first-year ice melt pond fraction in X-band SAR imagery". 2016c. In review.

Freeman, A. and Durden, S. L. "A three-component scattering model for polarimetric SAR data". *IEEE Transactions on Geoscience and Remote Sensing*, **36**(3): 963–973, May 1998.

Fung, A. K. *Microwave scattering and emission models and their applications*. Artech House Inc., Norwood, MA, USA, 1994.

Geldsetzer, T., Arkett, M., Zagon, T., Charbonneau, F., Yackel, J. J. and Scharien, R. K. "All-Season Compact-Polarimetry C-band SAR Observations of Sea Ice". *Canadian Journal of Remote Sensing*, **41**(5): 485–504, September 2015.

Gill, J. P. and Yackel, J. J. "Evaluation of C-band SAR polarimetric parameters for discrimination of first-year sea ice types". *Canadian Journal of Remote Sensing*, **38**(03): 306–323, June 2012.

Gill, J. P., Yackel, J. J. and Geldsetzer, T. "Analysis of consistency in first-year sea ice classification potential of C-band SAR polarimetric parameters". *Canadian Journal of Remote Sensing*, **39**(2): 101–117, June 2013.

Gogineni, S. P., Moore, R. K., Grenfell, T. C., Barber, D. G., Digby, S. and Drinkwater, M. "The effects of freeze-up and melt processes on microwave signatures". In *Microwave Remote Sensing of Sea Ice*, edited by F. D. Carsey, volume 68, pp. 329–341. American Geophysical Union, Washington, DC, USA, 1992.

Gupta, M., Barber, D. G., Scharien, R. K. and Isleifson, D. "Detection and classification of surface roughness in an Arctic Marchginal sea ice zone". *Hydrological Processes*, **28**(3): 599–609, January 2014.

Haas, C., Lobach, J., Hendricks, S., Rabenstein, L. and Pfaffling, A. "Helicopter-borne measurements of sea ice thickness, using a small and lightweight, digital EM system". *Journal of Applied Geophysics*, **67**(3): 234–241, March 2009.

Hajnsek, I., Pottier, E. and Cloude, S. R. "Inversion of surface parameters from polarimetric SAR". *IEEE Transactions on Geoscience and Remote Sensing*, **41**(4): 727–744, April 2003.

Hallikainen, M. and Winebrenner, D. P. "The physical basis for sea ice remote sensing". In *Microwave Remote Sensing of Sea Ice*, edited by F. Carsey, pp. 29–46. American Geophysical Union, Washington, DC, USA, 1992.

Han, H., Im, J., Kim, M., Sim, S., Kim, J., Kim, D.-j. and Kang, S.-H. "Retrieval of Melt Ponds on Arctic Multiyear Sea Ice in Summer from TerraSAR-X Dual-Polarization Data Using Machine Learning Approaches: A Case Study in the Chukchi Sea with Mid-Incidence Angle Data". *Remote Sensing*, **8**: 57, 2016.

Hanesiak, J. M., Yackel, J. J. and Barber, D. G. "Effect of Melt Ponds on First-Year Sea Ice Ablation - Integration of RADARSAT-1 and Thermodynamic Modelling". *Canadian Journal of Remote Sensing*, **27**(5): 433–442, October 2001.

Hibler, W. D. "Removal of aircraft altitude variation from laser profiles of the arctic ice pack". *Journal of Geophysical Research*, **77**(36): 7190–7195, December 1972.

Holt, B. and Digby, S. A. "Processes and imagery of first-year fast sea ice during the melt season". *Journal of Geophysical Research*, **90**(C3): 5045–5062, 1985.

Hossain, M., Yackel, J. J., Dabboor, M. and Fuller, M. C. "Application of a three-component scattering model over snow-covered first-year sea ice using polarimetric C-band SAR data". *International Journal of Remote Sensing*, **35**(5): 1786–1803, March 2014.

Hudier, E. and Tolzczuk-Leclerc, S. "Snow and sea ice roughness characterization from Quad-Pol H-A-alpha classes relative distribution". In *2013 IEEE International Geoscience and Remote Sensing Symposium - IGARSS*, pp. 2451–2454. Melbourne, VIC, Australia, 21-26 July, 2013.

Hudson, S. R., Granskog, M. A., Sundfjord, A., Randelhoff, A., Renner, A. H. H. and Divine, D. V. "Energy budget of first-year Arctic sea ice in advanced stages of melt". *Geophysical Research Letters*, **40**: 2679–2683, 2013.

Hughes, N. E., Wilkinson, J. P. and Wadhams, P. "Multi-satellite sensor analysis of fast-ice development in the Norske Øer Ice Barrier, northeast Greenland". *Annals of Glaciology*, **52**(57): 151–160, May 2011.

Isleifson, D., Langlois, A., Barber, D. G. and Shafai, L. "C-Band Scatterometer Measurements of Multiyear Sea Ice Before Fall Freeze-Up in the Canadian Arctic". *IEEE Transactions on geoscience and remote sensing*, **47**(6): 1651–1661, 2010.

Jeffries, M. O., Schwartz, K. and Li, S. "Arctic summer sea-ice SAR signatures, melt-season characteristics, and melt-pond fractions". *Polar Record*, **33**(185): 101–112, October 1997.

Kern, S., Brath, M. and Stammer, D. "Melt Ponds as Observed with a Helicopter-Borne, Multi-Frequency Scatterometer in the Arctic Ocean in 2007". In *Proc. of ESA Living Planet Symp.*. European Space Agency (ESA SP-686), Bergen, Norway, 28 June - 2 July, 2010.

Kim, D. J., Hwang, B., Chung, K. H., Lee, S. H., Jung, H. S. and Moon, W. M. "Melt pond mapping with high-resolution SAR: The first view". *Proceedings of the IEEE*, **101**: 748–758, 2013.

Komarov, A. S., Isleifson, D., Barber, D. G. and Shafai, L. "Modeling and Measurement of C-Band Radar Backscatter From Snow-Covered First-Year Sea Ice". *IEEE Transactions on Geoscience and Remote Sensing*, **53**(7): 4063–4078, July 2015.

Kwok, R. "Outflow of Arctic Ocean Sea Ice into the Greenland and Barents Seas: 1979-2007". *Journal of Climate*, **22**(9): 2438–2457, May 2009.

Kwok, R., Cunningham, G. F. and Nghiem, S. V. "A study of the onset of melt over the Arctic Ocean in RADARSAT synthetic aperture radar data". *Journal of Geophysical Research*, **108**(C11): 3363, 2003.

Kwok, R., Cunningham, G. F., Wensnahan, M., Rigor, I., Zwally, H. J. and Yi, D. "Thinning and volume loss of the Arctic Ocean sea ice cover: 2003–2008". *Journal of Geophysical Research*, **114**(C7), Julyl 2009.

Laxon, S. W., Giles, K. A., Ridout, A. L., Wingham, D. J., Willatt, R., Cullen, R., Kwok, R., Schweiger, A., Zhang, J., Haas, C., Hendricks, S., Krishfield, R., Kurtz, N., Farrell, S. and Davidson, M. "CryoSat-2 estimates of Arctic sea ice thickness and volume". *Geophysical Research Letters*, **40**(4): 732–737, February 2013.

Leach, R., ed. *Characterisation of Areal Surface Texture*. Springer, Berlin, Heidelberg, 2013.

Lee, J.-S. and Pottier, E. *Polarimetric radar imaging: From basics to applications*. CRC Press, Taylor and Francis Group, Boca Raton, FL, USA, 2009.

Livingstone, C., Onstott, R., Arsenault, L., Gray, A. and Singh, K. "Microwave Sea-Ice Signatures near the Onset of Melt". *IEEE Transactions on Geoscience and Remote Sensing*, **GE-25**(2): 174–187, March 1987.

MacDonald, D. and Ltd, A. "RADARSAT-2 Product Description". http://www.mdacorporation.com/docs/default-source/technical-documents/geospatial-services/r2_detailed_product_table.pdf?sfvrsn=4, visited 4 April 2016, March 2016.

Mahmud, M. S., Howell, S. E. L., Geldsetzer, T. and Yackel, J. J. "Detection of melt onset over the northern Canadian Arctic Archipelago sea ice from RADARSAT, 1997âĂŞ2014". *Remote Sensing of Environment*, **178**: 59–69, June 2016.

Mäkynen, M., Kern, S., Rösel, A. and Pedersen, L. T. "On the Estimation of Melt Pond Fraction on the Arctic Sea Ice With ENVISAT WSM Images". *IEEE Transactions on Geoscience and Remote Sensing*, **52**(11): 7366–7379, November 2014.

Mardia, K. V. "Measure of multivariate skewness and kurtosis with applications". *Biometrica*, **57**(3): 519–530, 1970.

Mattia, F., Le Toan, T., Souyris, J.-C., De Carolis, C., Floury, N., Posa, F. and Pasquariello, N. G. "The effect of surface roughness on multifrequency polarimetric SAR data". *IEEE Transactions on Geoscience and Remote Sensing*, **35**(4): 954–966, July 1997.

Meier, W. N., Hovelsrud, G. K., van Oort, B. E., Key, J. R., Kovacs, K. M., Michel, C., Haas, C., Granskog, M. A., Gerland, S., Perovich, D. K., Makshtas, A. and Reist, J. D. "Arctic sea ice in transformation: A review of recent observed changes and impacts on biology and human activity". *Reviews of Geophysics*, **52**(3): 185–217, September 2014.

Moen, M.-A. *Analysis and Interpretation of C-band Polarimetric SAR Signatures of Sea Ice*. Ph.D. thesis, UiT-The Arctic University of Norway, 2014.

Moen, M.-A., Doulgeris, A. P., Anfinsen, S. N., Renner, A. H. H., Hughes, N., Gerland, S. and Eltoft, T. "Comparison of feature based segmentation of full polarimetric SAR satellite sea ice images with manually drawn ice charts". *The Cryosphere*, **7**(6): 1693–1705, November 2013.

Moreira, A., Prats-Iraola, P., Younis, M., Krieger, G., Hajnsek, I. and Papathanassiou, K. P. "A tutorial on synthetic aperture radar". *IEEE Geoscience and Remote Sensing Magazine*, **1**(1): 6–43, March 2013.

Nakamura, K., Wakabayashi, H., Naoki, K., Nishio, F., Moriyama, T. and Uratsuka, S. "Observation of sea-ice thickness in the sea of Okhotsk by using dual-frequency and fully polarimetric airborne SAR (pi-SAR) data". *IEEE Transactions on Geoscience and Remote Sensing*, **43**(11): 2460–2469, November 2005.

Oliver, C. and Quegan, S. *Understanding Synthetic Aperture Radar Images*. Scitech Publishing, Inc, Raleigh, USA, 2004.

Onstott, R. G. "SAR and Scatterometer Signatures of Sea Ice". In *Microwave Remote Sensing of Sea Ice*, edited by F. Carsey, volume 68, pp. 73–104. American Geophysical Union, Washington, DC, USA, 1992.

Onstott, R. G. and Gogineni, S. P. "Active microwave measurements of Arctic sea ice under summer conditions". *Journal of Geophysical Research*, **90**(C3): 5035–5044, 1985.

Onstott, R. G., Grenfell, T. C., Matzler, C., Luther, C. A. and Svendsen, E. A. "Evolution of microwave sea ice signatures during early summer and midsummer in the Marchginal ice zone". *Journal of Geophysical Research*, **92**(C7): 6825–6835, 1987.

Parkinson, C. L. and Comiso, J. C. "On the 2012 record low Arctic sea ice cover: Combined impact of preconditioning and an August storm". *Geophysical Research Letters*, **40**(7): 1356–1361, April 2013.

Perovich, D. K. "Seasonal evolution of the albedo of multiyear Arctic sea ice". *Journal of Geophysical Research*, **107**: 1–13, 2002.

Perovich, D. K., Meier, W. N., Tschudi, M. A., Farrell, S., Gerland, S. and Hendricks, S. "Sea ice [in Arctic Report Card 2015]". URL: http://www.arctic.noaa.gov/reportcard, 2015.

Petrich, C. and Eicken, H. "Growth, Structure and Properties of Sea Ice". In *Sea Ice*, edited by D. N. Thomas and G. S. Dieckmann, pp. 23–77. Wiley-Blackwell, Oxford, UK, October 2009.

Polashenski, C., Perovich, D. and Courville, Z. "The mechanisms of sea ice melt pond formation and evolution". *Journal of Geophysical Research*, **117**(C1): C01001, January 2012.

Raney, R. K. "Hybrid-polarity SAR architecture". *Geoscience and Remote Sensing, IEEE Transactions on*, **45**(11): 3397–3404, 2007.

Raney, R. K. "A perspective on compact polarimetry". *IEEE Geosci. Remote Sens. Newslett.*, pp. 12–18, 2011.

Renner, A. H. H., Dumont, M., Beckers, J., Gerland, S. and Haas, C. "Improved characterisation of sea ice using simultaneous aerial photography and sea ice thickness measurements". *Cold Regions Science and Technology*, **92**: 37–47, August 2013a.

Renner, A. H. H., Hendricks, S., Gerland, S., Beckers, J., Haas, C. and Krumpen, T. "Large-scale ice thickness distribution of first-year sea ice in spring and summer north of Svalbard". *Annals of Glaciology*, **54**(62): 13–18, July 2013b.

Renner, A. H. H., Gerland, S., Haas, C., Spreen, G., Beckers, J. F., Hansen, E., Nicolaus, M. and Goodwin, H. "Evidence of Arctic sea ice thinning from direct observations". *Geophysical Research Letters*, **2012**: 1–8, 2014.

von Saldern, C., Haas, C. and Dierking, W. "Parameterization of Arctic sea-ice surface roughness for application in ice type classification". *Annals of Glaciology*, **44**: 224–230, 2006.

Scharien, R. K., Yackel, J. J., Granskog, M. A. and Else, B. G. "Coincident high resolution optical-SAR image analysis for surface albedo estimation of first-year sea ice during summer melt". *Remote Sensing of Environment*, **111**(2-3): 160–171, November 2007.

Scharien, R. K., Geldsetzer, T., Barber, D. G., Yackel, J. J. and Langlois, A. "Physical, dielectric, and C band microwave scattering properties of first-year sea ice during advanced melt". *Journal of Geophysical Research*, **115**(C12): C12026, December 2010.

Scharien, R. K., Yackel, J. J., Barber, D. G., Asplin, M., Gupta, M. and Isleifson, D. "Geophysical controls on C band polarimetric backscatter from melt pond covered Arctic first-year sea ice: Assessment using high-resolution scatterometry". *Journal of Geophysical Research: Oceans*, **117**(C9), September 2012.

Scharien, R. K., Hochheim, K., Landy, J. and Barber, D. G. "First-year sea ice melt pond fraction estimation from dual-polarisation C-band SAR – Part 2: Scaling in situ to Radarsat-2". *The Cryosphere*, **8**: 2163–2176, 2014a.

Scharien, R. K., Landy, J. and Barber, D. G. "First-year sea ice melt pond fraction estimation from dual-polarisation C-band SAR – Part 1: In situ observations". *The Cryosphere*, **8**: 2147–2162, 2014b.

Scheuchl, B., Hajnsek, I. and Cumming, I. "Model-based classification of polarimetric SAR sea ice data". In *IEEE International Geoscience and Remote Sensing Symposium (IGARSS '02) (Vol. 3)*, pp. 1521–1523. Toronto, Canada, 24-28 June, 2002a.

Scheuchl, B., Hajnsek, I. and Cumming, I. "Sea ice classification using multi-frequency polarimetric SAR data". In *IEEE International Geoscience and Remote Sensing Symposium (IGARSS '02) (Vol. 3)*, pp. 1914–1916. Toronto, Canada, 24-28 June, 2002b.

Scheuchl, B., Flett, D., Caves, R. and Cumming, I. "Potential of RADARSAT-2 data for operational sea ice monitoring". *Canadian Journal of Remote Sensing*, **30**(3): 448–461, January 2004.

Scheuchl, B., Cumming, I. and Hajnsek, I. "Classification of fully polarimetric single- and dual-frequency SAR data of sea ice using the Wishart statistics". *Canadian Journal of Remote Sensing*, **31**(1): 61–72, January 2005.

Schuler, D., Kasilingam, D. and Nesti, G. "Surface roughness and slope measurements using polarimetric SAR data". *IEEE Transactions on Geoscience and Remote Sensing*, **40**(3): 687–698, March 2002.

Shokr, M. and Nirmal, S. *Sea Ice: Physics and Remote Sensing*. John Wiley & Sons. Inc, Hoboken, USA, 2015.

Skrunes. *Characterization of low backscatter regions in the Marchine environment by multi-polarization C- and X-band synthetic aperure radar data*. Ph.d thesis, UiT - The Arctic University of Norway, 2014.

Skrunes, S., Brekke, C. and Eltoft, T. "Characterization of Marchine Surface Slicks by Radarsat-2 Multipolarization Features". *IEEE Transactions on Geoscience and Remote Sensing*, **52**(9): 5302–5319, September 2014.

Stroeve, J. C., Kattsov, V., Barrett, A., Serreze, M., Pavlova, T., Holland, M. and Meier, W. N. "Trends in Arctic sea ice extent from CMIP5, CMIP3 and observations". *Geophysical Research Letters*, **39**(16): L16502, August 2012.

Stroeve, J. C., Marchkus, T., Boisvert, L., Miller, J. and Barrett, A. "Changes in Arctic melt season and implications for sea ice loss". *Geophysical Research Letters*, **41**(4): 1216–1225, February 2014.

Torres, R., Snoeij, P., Geudtner, D., Bibby, D., Davidson, M., Attema, E., Potin, P., Rommen, B., Floury, N., Brown, M., Traver, I. N., Deghaye, P., Duesmann, B., Rosich, B., Miranda, N., Bruno, C., L'Abbate, M., Croci, R., Pietropaolo, A., Huchler, M. and Rostan, F. "GMES Sentinel-1 mission". *Remote Sensing of Environment*, **120**: 9–24, May 2012.

Tucker, W. B., Perovich, D. K., Gow, A. J., Weeks, W. F. and Drinkwater, M. R. "Pysical Properties of Sea Ice Relevant to Remote Sensing". In *Microwave Remote Sensing of Sea Ice*, edited by F. Carsey, pp. 9–28. American Geophysical Union, Washington, DC, USA, 1992.

Ulaby, F. T., Moore, R. K. and Fung, A. K. *Microwave Remote Sensing: Active and passive, Volume 3*. Artech House Inc., Norwood, MA, USA, 1986.

Ulaby, F. T., Long, D. G., Blackwell, W. J., Elachi, C., Fung, A. K., Ruf, C., Sarabandi, K., Zebker, H. A. and van Zyl, J. J. *Microwave Radar and Radiometric Remote Sensing*. University of Michigan Press, Ann Arbor, MI, USA, 2014.

Villano, M., Krieger, G. and Moreira, A. "Staggered SAR: High-Resolution Wide-Swath Imaging by Continuous PRI Variation". *IEEE Transactions on Geoscience and Remote Sensing*, **52**(7): 4462–4479, July 2014.

Wakabayashi, H., Matsuoka, T., Nakamura, K. and Nishio, F. "Polarimetric Characteristics of sea ice in the sea of Okhotsk observed by airborne L-band SAR". *IEEE Transactions on Geoscience and Remote Sensing*, **42**(11): 2412–2425, November 2004.

Warner, K., Iacozza, J., Scharien, R. k. and Barber, D. G. "On the classification of melt season first-year and multi-year sea ice in the Beaufort Sea using Radarsat-2 data". *International Journal of Remote Sensing*, **34**(11): 3760–3774, June 2013.

Winebrenner, D. P., Nelson, E. D., Colony, R. and West, R. D. "Observation of melt onset on multiyear Arctic sea ice using the ERS 1 synthetic aperture radar". *Journal of Geophysical Research*, **99**(C11): 22425–22441, 1994.

WMO. "Sea-ice nomenclature and interational system of sea ice symbols". Technical report, World Meteorological Organisation, Geneva, Switzerland, 2014.

Wolf, E. "Coherence properties of partially polarized electromagnetic radiation". *Il Nuovo Cimento*, **13**: 1165–1181, 1959.

Yackel, J. J. and Barber, D. G. "Melt ponds on sea ice in the Canadian Archipelago: 2. On the use of RADARSAT-1 synthetic aperture radar for geophysical inversion". *Journal of Geophysical Research*, **105**(C9): 22061–22070, 2000.

Yackel, J. J., Barber, D. G. and Papakyriakou, T. N. "On the estimation of spring melt in the North Water polynya using RADARSAT-1". *Atmosphere-Ocean*, **39**(3): 195–208, September 2001.

Yackel, J. J., Barber, D. G., Papakyriakou, T. N. and Breneman, C. "First-year sea ice spring melt transitions in the Canadian Arctic Archipelago from time-series synthetic aperture radar data, 1992-2002". *Hydrological Processes*, **21**(2): 253–265, January 2007.

van Zyl, J. J. and Kim, Y. *Synthetic Aperture Radar Polarimetry*. John Wiley & Sons, Inc, Hoboken, USA, 2011.